UCLA
UCLA Previously Published Works

Title
Injectable polypeptide hydrogels via methionine modification for neural stem cell delivery

Permalink
https://escholarship.org/uc/item/6t95t9zg

Authors
Wollenberg, AL
O'Shea, TM
Kim, JH
et al.

Publication Date
2018-09-01

DOI
10.1016/j.biomaterials.2018.03.057

Peer reviewed

eScholarship.org Powered by the California Digital Library
University of California

Author Manuscript

Author Manuscript

Author Manuscript

Author Manuscript

HHS Public Access

Author manuscript

Biomaterials. Author manuscript; available in PMC 2019 September 01.

Published in final edited form as:

Biomaterials. 2018 September ; 178: 527–545. doi:10.1016/j.biomaterials.2018.03.057.

Injectable polypeptide hydrogels via methionine modification for neural stem cell delivery

A.L. Wollenberg[1,*], **T.M. O'Shea**[2,*], **J.H. Kim**[2], **A. Czechanski**[3], **L.G. Reinholdt**[3], **M.V. Sofroniew**[2], and **T.J. Deming**[1,†]

[1]Departments of Bioengineering, Chemistry and Biochemistry, University of California, Los Angeles, Los Angeles, California 90095-1600, USA

[2]Department of Neurobiology, David Geffen School of Medicine, University of California, Los Angeles, California 90095-1763, USA

[3]The Jackson Laboratory, Bar Harbor, Maine, 04609, USA

Abstract

Injectable hydrogels with tunable physiochemical and biological properties are potential tools for improving neural stem/progenitor cell (NSPC) transplantation to treat central nervous system (CNS) injury and disease. Here, we developed injectable diblock copolypeptide hydrogels (DCH) for NSPC transplantation that contain hydrophilic segments of modified L-methionine (Met). Multiple Met-based DCH were fabricated by post-polymerization modification of Met to various functional derivatives, and incorporation of different amino acid comonomers into hydrophilic segments. Met-based DCH assembled into self-healing hydrogels with concentration and composition dependent mechanical properties. Mechanical properties of non-ionic Met-sulfoxide formulations (DCH_{MO}) were stable across diverse aqueous media while cationic formulations showed salt ion dependent stiffness reduction. Murine NSPC survival in DCH_{MO} was equivalent to that of standard culture conditions, and sulfoxide functionality imparted cell non-fouling character. Within serum rich environments *in vitro*, DCH_{MO} was superior at preserving NSPC stemness and multipotency compared to cell adhesive materials. NSPC in DCH_{MO} injected into uninjured forebrain remained local and, after 4 weeks, exhibited an immature astroglial phenotype that integrated with host neural tissue and acted as cellular substrates that supported growth of host-derived axons. These findings demonstrate that Met-based DCH are suitable vehicles for further study of NSPC transplantation in CNS injury and disease models.

TOC image

†Corresponding Author.
*These authors contributed equally to this work.

Publisher's Disclaimer: This is a PDF file of an unedited manuscript that has been accepted for publication. As a service to our customers we are providing this early version of the manuscript. The manuscript will undergo copyediting, typesetting, and review of the resulting proof before it is published in its final citable form. Please note that during the production process errors may be discovered which could affect the content, and all legal disclaimers that apply to the journal pertain.

Author Manuscript Author Manuscript Author Manuscript Author Manuscript

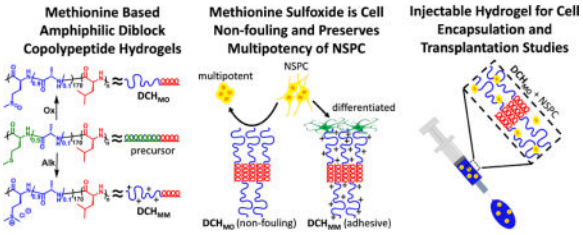

Keywords

biomaterials; polypeptides; hydrogels; neural stem cells; brain; cell transplantation

1. Introduction

Transplantation of neural stem/progenitor cells (NSPC) has emerged as a potential therapy for treatment of central nervous system (CNS) diseases and injuries including Parkinson's, spinal cord injury, and stroke[1]. NSPC can be readily derived from embryonic[2,3], adult[4–6], and induced pluripotent stem (iPS) sources[7] and upon transplantation *in vivo* show a capacity to differentiate into glial and neuronal phenotypes that can integrate into host circuitry[8,9]. In the context of injury or disease, NSPC grafting has aided host neuronal survival, axon regeneration, remyelination and traumatic lesion re-vascularization[10]. However, despite their promise, NSPC therapies face considerable challenges including: (i) widespread cell graft necrosis and apoptosis[11,12], (ii) inappropriate differentiation and cell fate decision making, (iii) cellular migration away from lesioned/diseased neural tissue resulting in ectopic colonies along the brain and spinal cord neuroaxis, and (iv) isolation of cell grafts away from adjacent viable neural tissue by graft induced inflammation and fibrosis[6,13,14]. Inability to address these challenges limits the functional potential of NSPC transplantation and hampers clinical translation. NSPC transplantation would benefit from innovative bioengineering strategies that: (1) enhance survival of injected cells; (2) direct progenitor differentiation *in vivo;* and (3) optimize graft-host interactions. Injectable hydrogel carriers have emerged as potential tools to aid NSPC transplantation. To date, fibrin gels have been the predominant material of choice in NSPC grafting studies due to their commercial availability and straight forward formulation[15–17]. However, the limited control over physical, chemical and mechanical properties of fibrin gels and their inherent and uncontrollable bioactivity has prompted efforts to develop alternative synthetic hydrogels for NSPC transplantation[18,19].

To identify hydrogel properties that influence NSPC transplantation outcomes we and others have been focused on engineering injectable synthetic hydrogels with robust tunability of physiochemical and biological properties. For example, blends of hyaluronan and methylcellulose have demonstrated utility in enhancing the survival of grafted NSPCs in models of spinal cord injury[20], retinal disease and stroke[21]. In these studies, a rigorous mechanistic investigation uncovered a pro-survival effect of the inclusion of bioactive hyaluronan, which was attributed to its high affinity for CD44 receptors on progenitor cells[21]. Variations in methylcellulose concentration also allowed for manipulation of hydrogel mechanical properties, which influenced the injectability and overall survival of

Author Manuscript Author Manuscript Author Manuscript Author Manuscript

transplanted NSPC using this system. Other studies using an elastin-like protein based hydrogel established that the progenitor state of NSPC is modulated by the stiffness and degradability of the suspending matrix[22].

We have developed biomimetic hydrogels for drug delivery and cell transplantation using synthetic polypeptides. Polypeptide hydrogels are versatile materials that can: (i) be enzymatically degraded, (ii) include a wide range of chemical functionality, (iii) adopt ordered conformations that can drive structural and mechanical properties, and (iv) respond to biological stimuli[1,23]. Our synthetic materials are based on amphiphilic diblock copolypeptide hydrogels (DCH) that in their first iteration were composed of discrete hydrophobic and ionic hydrophilic segments (e.g. poly(L-lysine·HCl)$_{180}$-*block*-poly(L-leucine)$_{20}$, **K$_{180}$L$_{20}$** or DCH$_K$)[24,25], and possessed many features attractive for CNS applications[26,27]. DCH are physically associated gels composed of branched and tangled nanoscale tape-like assemblies that can be deformed by applied stress and injected through narrow diameter cannulae, after which they rapidly re-assemble into elastic gel networks[24,25]. When injected into mouse CNS tissues, ionic DCH self-assemble into discrete, well-formed deposits of rigid gel networks *in vivo* that integrate well with host CNS tissue, causing no detectable toxicity, and are fully degraded *in vivo*[27]. We also reported both *in vitro* and *in vivo* evidence that ionic DCH can serve as depots for sustained local release of both hydrophilic and hydrophobic effector molecules for investigative and potential therapeutic applications in the CNS[26].

Although they have many advantageous properties as hydrogels *in vivo*, one limitation of ionic DCH is their cytotoxicity towards cells encapsulated completely within the material matrix[28], which precludes their use in cell grafting applications. To obtain cell-compatible hydrogels, we focused on creating non-ionic DCH, since non-ionic polymers and hydrogels are well known to be less toxic to cells *in vitro*[29]. In an initial proof of concept study, we developed DCH containing non-ionic poly(γ-[2-(2-methoxyethoxy)ethyl]-*rac*-glutamate), ***rac*-E^{P2}**, hydrophilic segments instead of charged polypeptide segments, and found the resulting hydrogels, termed DCH$_{EO}$, retained the advantageous physical properties of ionic DCH, as well as displayed no significant cytotoxicity to either mesenchymal stem cells or NSPC for periods up to 7 days *in vitro*. Furthermore, DCH$_{EO}$ demonstrated improved cell viability, localization and host integration of NSPC grafted into crush spinal cord injury lesions compared to that afforded by culture media alone[28]. The enhanced performance was attributed to superior suspension of the NSPCs and a more even distribution of grafted cells within the SCI lesion afforded by DCH$_{EO}$. While DCH$_{EO}$ are promising as cell carriers, the chemistry of the ***rac*-E^{P2}** component limits the further development and utility of these hydrogels. In addition to being composed of unnatural amino acids that require additional synthesis steps and purification, hydrolysis of side-chain linkages may lead to premature degradation of the DCH$_{EO}$ in aqueous media. The reactivity of side-chain ester linkages also prohibits the incorporation of other protected functional monomers into DCH$_{EO}$, since most deprotection conditions will also cleave off the diethylene glycol chains from the glutamate residues.

In the study presented here, we sought to overcome the synthesis and functionality limitations associated with DCH$_{EO}$ by utilizing new methods for post-polymerization

Author Manuscript Author Manuscript Author Manuscript Author Manuscript

modification of L-methionine (Met) residues in copolypeptides[30] to enable scalable synthesis and add new capabilities beyond those in DCH_{EO}. Met is an essential amino acid in living systems with rich biochemistry. For example, Met residues can be selectively alkylated to give sulfonium salt derivatives that allow for the introduction of ionic groups in polypeptides[31,32]. This chemistry has been used to convert hydrophobic, α-helical poly(L-methionine), **M**, into a wide variety of water soluble, ionic poly(S-alkyl-L-methionine sulfonium)s, $\mathbf{M^R}$, containing diverse functionality[33]. Alternatively, Met residues can also be readily and selectively oxidized to give highly polar, non-ionic L-methionine sulfoxide, MetO, residues[34–36]. Polymers containing MetO residues have shown interesting physiochemical and biological properties that may be advantageous for their use in hydrogels for NSPC transplantation[37–41]. For example, membranes of poly(L-methionine sulfoxide), $\mathbf{M^O}$, demonstrated enhanced water permeability compared to parent, non-oxidized, **M** polymers[37,38], as well as improved solubility and transport of hydrophilic polypeptide drugs and hydrophobic small molecules[39]. Furthermore, $\mathbf{M^O}$ chains have been found to exhibit negligible diffusion across cell membranes, and sulfoxide groups in polymers and on surfaces have been found to impart inherent resistance against protein adsorption. The mechanism of this exceptional protein and cell non-fouling character has been attributed to the capacity of sulfoxide groups to act as hydrogen bond acceptors but not donors, analogous to how ethylene oxide groups contribute to protein adsorption resistance in polyethylene glycol based materials[42–44]. These characteristics suggest that $\mathbf{M^O}$ may be an excellent component for biomaterial formulations with negligible *in vitro* or *in vivo* cytoxicity[41,45–47]. Additionally, since biological systems contain catabolic enzymatic mechanisms to readily reduce MetO residues in proteins back to Met, and we have shown $\mathbf{M^O}$ polymer can be readily degraded by proteolytic enzymes *in vitro*[40], $\mathbf{M^O}$ based biomaterials should be readily and safely resorbed *in vivo*[48].

Given the numerous advantages described above, both alkylated and oxidized **M** chains represent potentially attractive candidates as hydrophilic segments in DCH intended for use in NSPC grafting applications. The abundance and low cost of the precursor Met amino acid, the ease of synthesis and purification of Met NCA monomer, and high yield polymerization and post-polymerization modification reactions[49] allow the modified Met-based DCH platform to be readily scalable and amenable to being manufactured in compliance with GMP standards that would be required for human use. Here, we outline the design and synthesis of modified Met-based DCH materials, demonstrate the tunable physiochemical and biological properties achieved through post-polymerization modifications of the Met residues, and establish the utility of specific formulations of Met-sulfoxide based DCH_{MO} for NSPC transplantation applications.

2. Materials and Methods

2.1. Synthesis and characterization of copolypeptides

2.1.1. Materials and Instrumentation—Tetrahydrofuran (THF), hexanes, and methylene chloride were dried by purging with nitrogen and passage through activated alumina columns prior to use. Triethylamine (TEA) and trimethylsilyl chloride (TMSCl) were purified by distillation and stored over 3 Å molecular sieves. $Co(PMe_3)_4$, L-

Author Manuscript Author Manuscript Author Manuscript Author Manuscript

methionine, L-leucine, and L-alanine amino acid N-carboxyanhydride (NCA) monomers were prepared according to literature procedures[27,49,50]. All other chemicals were purchased from commercial suppliers and used without further purification unless otherwise noted. Selecto silica gel 60 (particle size 0.032–0.063 mm) was used for flash column chromatography. Fourier Transform Infrared (FTIR) measurements were taken on a Perkin Elmer RX1 FTIR spectrophotometer calibrated using polystyrene film, and attenuated total reflectance infrared (ATR-IR) data were collected using a PerkinElmer Spectrum 100 FTIR spectrometer equipped with a universal ATR sample accessory. ^{1}H NMR spectra were acquired on a Bruker ARX 400 spectrometer. Tandem gel permeation chromatography/light scattering (GPC/LS) was performed at 25 °C using an SSI Accuflow Series III pump equipped with Wyatt DAWN EOS light scattering and Optilab REX refractive index detectors. Separations were achieved using 100 Å and 1000 Å PSS-PFG 7 μm columns at 30 °C with 0.5% (w/w) KTFA in 1,1,1,3,3,3-hexafluoroisopropanol (HFIP) as eluent and sample concentrations of 10 mg/ml. Pyrogen free deionized water (DI) was obtained from a Millipore Milli-Q Biocel A10 purification unit. Dialysis was conducted using regenerated cellulose dialysis tubing (Spectrum Labs).

2.1.2. Preparation of N-Boc-L-lysine NCA—The preparation of N-Boc-L-lysine NCA was modified from a procedure in literature[51]. To a solution of N-Boc-L-lysine amino acid (1 equiv) in dry THF (0.15 M) in a Schlenk flask was added TEA (2 equiv) and TMSCl (2 equiv) via syringe. The reaction was stirred under N_2 at 20 °C for 1 hour. Upon addition of TEA and TMSCl, precipitation of TEA·HCl was observed. Phosgene solution in toluene (15% (w/v), 2 equiv) was then added via syringe and the reaction was stirred under N_2 at 50 °C for 2 hours. *Caution!* Phosgene is extremely hazardous and all manipulations must be performed in a well-ventilated chemical fume hood with proper personal protection and necessary precautions taken to avoid exposure. After 2 hours, the reaction was evaporated to dryness and transferred into a N_2 filled glovebox. In the fume hood, the condensate in the Schlenk line vacuum traps was treated with 50 mL of concentrated aqueous NH_4OH to neutralize residual phosgene. In the glove box, the insoluble TEA·HCl was removed by dissolving the product in 30% THF in hexanes and passing through a plug of vacuum dried silica[49]. The combined NCA containing fractions were dried under reduced pressure and the product was dissolved in a minimal amount of THF and crystallized by addition of hexanes (1:3 THF:hexanes). Multiple crystallizations (5×) were required for adequate NCA purification (overall yield = 52%). ^{1}H NMR and FTIR spectral data were consistent with previously reported values from literature[52].

2.1.3. General Copolypeptide Synthetic Procedure—All polymerization reactions were performed in a N_2 filled glove box using anhydrous solvents. To prepare copolypeptide at *ca.* 100 mg scale, a solution of $Co(PMe_3)_4$ (4.5 mg, 0.012 mmol) in THF (20 mg/mL) was quickly added to a solution of L-methionine NCA (Met NCA; 100 mg, 0.57 mmol) and L-alanine NCA (Ala NCA; 7.3 mg, 0.063 mmol) in THF (50 mg/mL). To synthesize lysine containing copolypeptides, Ala NCA in the above procedure was replaced with N-Boc-L-lysine NCA (Boc-Lys NCA) at the desired molar ratio. After *ca.* 60 min., complete consumption of NCA was confirmed by FTIR spectroscopy. In order to determine the lengths of poly(L-methionine-*stat*-L-alanine), **MA**, or poly(L-methionine-*stat*-Boc-L-

Author Manuscript Author Manuscript Author Manuscript Author Manuscript

lysine), **MK^{Boc}**, segments, a small aliquot (200 μl) of each polymerization mixture was removed for end-group analysis (*vide infra*). To each remaining copolymerization mixture was then added L-leucine NCA (Leu NCA; 5.9 to 20 mg, 0.038 to 0.13 mmol) in THF (50 mg/mL). The Leu NCA monomers were found to be completely consumed within *ca*. 60 min., and the reaction mixtures were subsequently removed from the glove box. The block copolypeptide solutions were then precipitated by addition to a 0.1 M aqueous HCl solution (75 mL), filtered, washed with DI water, and dried under reduced pressure to yield white fluffy solids with yields ranging from 90 to 95%. Detailed compositional and characterization data for all samples are provided in the Supplementary Information.

2.1.4. Sample procedure for MA$_m$ chain length determination using end-group analysis—In the glove box, α-methoxy-ω-isocyanoethyl-poly(ethylene glycol)$_{23}$ (mPEG$_{23}$-NCO)[53] (20 mg) was dissolved in THF (1 ml) in a 20 ml scintillation vial. An aliquot (200 μl) of copolymerization solution containing active chain ends (from 2.1.3 above) was removed and added to the solution of mPEG$_{23}$-NCO. The PEG end-capped sample (e.g. **MA$_m$-mPEG$_{23}$**) was sealed, allowed to stir for 24 h, and then used for chain length determination. Outside of the glove box, the PEG end-capped sample was washed with 10 mM aqueous HCl (2×). After stirring for 1 h, **MA$_m$-mPEG$_{23}$** was collected by centrifugation and washed with DI water (3 × 20 ml) to remove all non-conjugated mPEG$_{23}$-NCO. The remaining **MA$_m$-mPEG$_{23}$** was then freeze-dried to remove residual H_2O. To determine **MA$_m$** molecular weights (M_n), ^{1}H NMR spectra were obtained. Since it has been shown that end-capping is quantitative for $(PMe_3)_4Co$ initiated NCA polymerizations when excess isocyanate is used[53], integrations of methionine (δ 2.70) and alanine (δ 1.52) resonances versus the polyethylene glycol resonance at δ 3.92 could be used to obtain both the ratios of **M** to **A** and **MA$_m$** lengths.

2.1.5. Procedure for Oxidation of Met Residues in Copolypeptides—For Boc-Lys containing copolypeptides, deprotection was performed before oxidation of Met residues (see 2.1.7). To convert Met residues in copolypeptides to Met sulfoxide residues, a volume of 70 wt. % *tert*-butyl hydroperoxide (TBHP) (16 molar equivalents per Met residue) was added to a sample of solid copolypeptide (ca. 80 mg). The reaction mixture was then diluted with DI water to yield an overall polypeptide concentration of *ca*. 20 mg/mL. To aid oxidation, a catalytic amount of camphorsulfonic acid (CSA) (0.2 molar equivalents per Met residue) solution in DI water (20 mg/ml) was subsequently added. The reaction mixture was stirred vigorously for 24 hours at ambient temperature, whereupon complete dissolution of copolypeptide samples was observed. Reaction mixtures were transferred to 2000 MWCO dialysis bags and dialyzed against: (i) pyrogen free deionized milli-Q water (3.5L) containing sodium thiosulfate (1.2 g, 2.16 mM) for 2 days to neutralize residual peroxide, (ii) milli-Q water (3.5L) acidified to pH 4 with HCl for 2 days to aid cobalt ion removal, and (iii) milli-Q water (3.5L) for 2 days to remove residual HCl. For each step dialysate was changed every 12 hours. Copolypeptide solutions were then freeze dried to yield white fluffy solids with average yields of 90 to 95%, and 100% conversion of Met residues to Met sulfoxide groups.

Author Manuscript Author Manuscript Author Manuscript Author Manuscript

2.1.6. Procedure for Methylation of Met Residues in Copolypeptides—To convert Met residues in copolypeptides to S-methyl-Met sulfonium residues, iodomethane (3 equivalents per Met residue) was added to suspensions of copolypeptides (ca. 80 mg) in DI water (*ca.* 20 mg/ml). Reaction mixtures were covered with aluminum foil to protect iodomethane from light, and then stirred vigorously for 5 days at ambient temperature. After 5 days, reaction mixtures were found to be suspensions of particulates. The copolypeptides were subsequently transferred to 2000 MWCO dialysis bags and dialyzed against: (i) pyrogen free deionized milli-Q water (3.5L) containing sodium metabisulfite (0.50 g, 0.75 mM) for 1 day to remove iodine based impurities, (ii) milli-Q water (3.5L) acidified to pH 4 for 2 days to aid cobalt ion removal, (iii) milli-Q water containing NaCl (7.0 g, 35 mM) for 2 days to facilitate iodide to chloride counterion exchange, and (iv) milli-Q water (3.5L) for 2 days to remove residual NaCl. For each step dialysate was changed every 12 hours. After dialysis all copolypeptides were completely soluble in DI water. Copolypeptide solutions were then freeze dried to yield white fluffy solids with average yields of 95 to 99%, and 99% conversion of Met residues to S-methyl-Met sulfonium groups.

2.1.7. Deprotection of Boc-Lys containing copolypeptides—Deprotection of Boc-Lys was performed before oxidation of Met residues. To facilitate deprotection, Boc-Lys containing copolypeptides (ca. 80 mg) were fully dissolved in trifluoroacetic acid (*ca.* 25 mg/mL) and stirred at ambient temperature for 2 hours. Copolypeptide samples were then precipitated into diethyl ether (75 mL). The diethyl ether was decanted away and the copolypeptides were dried under reduced pressure overnight to yield white solids (*ca.* 99% yield, 100% deprotection efficiency).

2.1.8. Preparation of DCH Formulations—DCH were prepared by solubilizing lyophilized copolypeptide in either DI water, phosphate buffered saline (PBS), or cell culture media and allowing to assemble for 24 hours, without stirring, before use.

2.1.9. Circular Dichroism—All circular dichroism spectra were collected using an OLIS RSM CD spectrophotometer (OLIS, USA) using conventional scanning mode. Poly(L-methionine sulfoxide), $\mathbf{M^O}$, and poly(L-methionine sulfoxide-*stat*-L-alanine), $\mathbf{M^OA}$, samples were characterized by recording spectra (185-260 nm) within a quartz cuvette of 0.1 cm path length. Samples were prepared at concentrations of 0.10 to 0.17 mg/mL in Milli-Q water. The spectra are reported in units of molar ellipticity [θ] (deg $cm^2 \cdot dmol^{-1}$), which was calculated using $[\theta] = (\theta \times 100 \times M_W)/(c \times l)$ where θ is the measured ellipticity (millidegrees), MW is the average residue molecular mass (g/mol), c is the polypeptide concentration (mg/mL), and l is the cuvette path length (cm).

2.2. DCH Characterization

2.2.1. Dynamic Mechanical Rheology—Dynamic rheological measurements were performed at constant set temperature of 25 °C using a Physica MCR 301 (Anton Paar, Sweden) equ ipped with a 25 mm 1° cone and plate geometry. To determine the linear viscoelastic testing region for each DCH sample a frequency sweep from 0.1 to 100 rad s^{-1} at a fixed strain of 0.5% was applied followed by a strain sweep from 0.1 to 100% strain at a fixed frequency of 10 rad s^{-1}. DCH samples were allowed to recover for a period of 2

Author Manuscript Author Manuscript Author Manuscript Author Manuscript

minutes between individual rheological experiments. To compare mechanical properties across various DCH samples a time sweep under fixed strain and frequency conditions (0.5% strain and 10 rad s^{-1}) was applied for one minute. To evaluate shear thinning and recovery behavior of DCH the strain amplitude parameters were stepped from 0.5% to 1000%, maintained at 1000% for 2 minutes and then returned to 0.5% to evaluate the recovery of the mechanical properties at a fixed frequency of 10 rad s^{-1}.

2.3. *In vitro* cell culture

2.3.1. Neural stem/progenitor cell (NSPC) derivation and culture—Neural stem/progenitor cells (NSPC) used in this study were derived from mouse embryonic stem cells (mESC). The mESC lines used in this study contain a Ribotag (a modified ribosomal protein L22 (Rpl22) with hemagglutinin epitope tag)[54] allele. The mESC lines were derived from the inner cell mass of E3.5 blastocyst stage embryos generated from crosses of male homozygous B6N.129-Rpl22tm1.1Psam/J(StockNo: 011029) “Ribotag” mice to females hemizygous for a dominant, maternal effect cre allele, B6.Cg-Tg(SOX2-cre)1Amc/J (StockNo: 008454) and heterozygous for the “Ribotag” allele. Multiple male and female mESC lines were derived, and each was karyotyped and genotyped to confirm sex and homozygosity for the cre-exised, Ribotag allele. For generation of NSPC an induction and expansion method reported widely within the literature was used[55–57]. Briefly, mESC were maintained and expanded on gelatin-coated plates in DMEM media containing a cocktail of supporting growth factors including Leukemia inhibitory factor (LIF) (EMD Millipore, Burlington, MA), ES grade Fetal Bovine Serum (FBS), nucleosides, non-essential amino acids and β-mercaptoethanol (Thermofisher Scientific). The neural induction of mESC was performed using a 2−/4+ protocol described in detail previously[55]. Specifically, 2×10^6 mESC were cultured for two days in LIF free differentiation media (Advanced DMEM/F12 media supplemented with knockout serum (Thermofisher Scientific), glutamine, nucleosides, non-essential amino acids and β-mercaptoethanol) under non-adherent suspension conditions to promote the formation of embryoid bodies (EB). After two days the EBs were transferred to gelatin coated flasks and cultured for four days in differentiation media supplemented with 50 nM retinoic acid (RA) and 500nM purmorphamine (PUR) (sonic hedgehog (SHH) agonist) to caudalize and neurally induce (NI) the cells[55]. Differentiation media with the RA/PUR morphogens was replaced after two days. Following neural induction the cells were subsequently expanded for several passages in neural progenitor cell media (Advanced DMEM/F12 supplemented with B27 (Thermofisher Scientific), nucleosides, non-essential amino acids, heparin and FGF/EGF (Peprotech) both at 100 ng/ml) to generate a population of definitive NSPC for *in vitro* studies. NSPC stocks that had undergone 15-24 passages (5-8 weeks of neural expansion) were used for experimental studies.

2.3.2. In vitro DCH NSPC viability evaluation—To evaluate hydrogel cytotoxicity, NSPC were suspended within DCH formulations and placed on top of 1% agarose molds containing unsupplemented Advanced DMEM/F12 media to ensure maintenance of hydrogel hydration. For each formulation 5000 cells/μL of hydrogel were suspended within the material and 30 μL of hydrogel/cell solution was added on top of the agarose molds. Each hydrogel sample was studied in triplicate. After 24 hours of incubation, hydrogels were

Author Manuscript Author Manuscript Author Manuscript Author Manuscript

thinned into liquids by dilution into 100 μL of 1× PBS containing 2 μM Calcein AM to identify viable cells and 4 μM EthD-1 to identify dead cells and allowed to incubate at room temperature for 30 minutes. Cell solutions were then transferred to glass slides, coverslipped and imaged using the FITC and Rhodamine filters on an epi-fluorescent microscope (Zeiss). At least five images per slide were collected resulting in a total of 15 images per hydrogel sample. Cell viability was normalized to the viability of cells incubated in media alone.

2.3.3. NSPC adhesion to DCH coated substrates—Hydrophobic, siliconized circular glass coverslips (12mm) (Hampton Research, Aliso Viejo, CA) or black 96 well untreated polystyrene plates (Brand, Germany) were coated with an appropriate volume of 0.1 wt% copolypeptide solubilized in 70% ethanol. After being allowed to adsorb for 1 hour, copolypeptide solutions were aspirated and the coated surfaces allowed to dry for 1 hour under ambient conditions. Before plating the cells, coated surfaces were washed once with water to remove any non-adsorbed copolypeptide. Cells were seeded at 200,000 and 100,000 cells for the coverslips and wells respectively and incubated on coated surfaces for 24 hours before analysis. For the coated coverslips, the cells were imaged under brightfield conditions using an EVOS XL cell imaging system (Thermofisher Scientific). After the 24 hour incubation period the 96 well plate was washed once with 1× PBS to remove non-adhered cells and the plate was then treated with 1× PBS containing 2 μM Calcein AM and 4 μM EthD-1 for 30 minutes to identify viable cells that remained adhered to the plate. The 96 well plate was read on a VICTOR 2V Multilabel fluorescent plate reader (Perkin Elmer). Quantification of cell attachment was normalized to a gelatin coated substrate which demonstrated the highest extent of cell adhesion.

2.3.4. NSPC differentiation on DCH substrates—To study the influence of cellular substrate interactions on NSPC differentiation outcomes, 100 mm non-treated polystyrene petri dishes were coated separately with DCH_{MO}, DCH_{MM} or gelatin. As in the adhesion experiments above, a 0.1 wt% copolypeptide solubilized in 70% ethanol was applied to each petri dish, allowed to incubate and dry for 1 hour and then washed once with water to remove non-adsorbed material. NSPC were seeded at a 2×10^6 cells/plate and cultured for 48 hours in media containing 10% FBS. After 48 hours cells were trypsinized and re-seeded on gelatin coated coverslips and cultured for an additional 72 hours in supplement free media to promote spontaneous differentiation.

2.3.5. Immunocytochemistry—Cell seeded coverslips were washed with 1× PBS and fixed for 30 minutes with 4% paraformaldehyde. Coverslips were then washed with TBS buffer, blocked and permeabilized with donkey serum and Triton X-100 in TBS buffer before being stained overnight with primary antibodies. Primary antibodies used within the *in vitro* experiments included: (i) rat anti mouse-GFAP (Thermofisher, #13-0300, 1:1000 dilution) (ii) rabbit anti mouse-TUJ-1 (Sigma, #T2200, 1:1000 dilution), (iii) goat anti-mouse-HA (Novus, NB600-362, 1:1000 dilution), (iv) rabbit anti-mouse HA (Sigma, H6908, 1:1000 dilution), (v) goat anti-mouse SOX2 (R&D Systems, AF2018, 1:300 dilution), (vi) goat anti-mouse SOX9 (Novus, H00006662-M02,1:200 dilution) (vii) chicken anti-mouse NESTIN (Novus, NB100-1604, 1:500 dilution). Fluorophore-conjugated secondary donkey antibodies (Jackson ImmunoResearch) raised against the various primary

Author Manuscript Author Manuscript Author Manuscript Author Manuscript

antibody species were applied for 2 hours. Coverslips were subsequently stained for DAPI and mounted on glass slides.

2.3.6. PCR—NSPCs were seeded on DCH_{MO}, DCH_{MM} or gelatin coated 100 mm non-treated polystyrene petri dishes at 6×10^6 cells per plate and cultured in NSPC media containing 10% FBS. At 48 hours cells were lysed and mRNA isolated using the RNEasy® Plus Mini RNA purification kit (Qiagen) following the manufacturer's instructions. Isolated mRNA was quantified by UV/VIS and 500ng of mRNA was used to synthesize cDNA using the iScript™ Reverse Transcription Supermix reagent (Biorad). qPCR was performed as a 10 μL reaction volume in a 96 well PCR plate on a Lightcycler 96 instrument (Roche) and incorporating SsoAdvanced™ Universal SYBR® Green Supermix (Biorad) and various primers (Supplementary Table 1). Relative gene expression was determined by comparing Δct values for each experimental condition that were normalized to the Ribotag (HA) gene expression.

2.4. *In vivo* DCH injections

2.4.1. Surgery—All surgical procedures used adhere to a protocol approved by the UCLA animal research committee. Wildtype C57BL/6 mice (8-12 weeks) were used for all experiments. For DCH injections, mice were anesthetized using isoflurane and a craniotomy performed using a high speed surgical drill. A volume of 1 μL of DCH was injected into the caudate putamen nucleus at 0.15 μL/min using target coordinates relative to Bregma: +0.5 mm A/P, +2.5mm L/M and −3.0 mm D/V. DCH injections were made using pulled glass micropipettes ground to a beveled tip with 150–250 μm inner diameter attached via specialized connectors and high-pressure tubing to a 10 μL syringe that was mounted to a stereotaxic frame and controlled by an automated microdrive pump.

2.4.2. Immunohistochemistry—At 4 weeks after hydrogel injection mice underwent transcardial perfusion with heparinized saline and 4% paraformaldehyde (PFA), and the brain was excised for histological analysis. Following an 8 hour post fixation in 4% PFA and a 72hr incubation in 30% sucrose, 40 μm coronal sections of brain were prepared using a cryostat. Tissue sections were stained as free floating sections using standardized immunohistochemistry techniques described by us elsewhere[26]. Specific antibodies used to stain brain tissue sections included: (i) rat anti mouse-GFAP (Thermofisher, #13-0300, 1:1000 dilution) (ii) rabbit anti mouse-TUJ-1 (Sigma, #T2200, 1:1000 dilution), (iii) goat anti-mouse-HA (Novus, NB600-362, 1:1000 dilution), (iv) rabbit anti-mouse HA (Sigma, H6908, 1:1000 dilution), (v) goat anti-mouse SOX2 (R&D Systems, AF2018, 1:300 dilution), (vi) goat anti-mouse SOX9 (Novus, H00006662-M02,1:200 dilution), (vii) goat anti-mouse NESTIN (R&D Systems, AF2736, 1:800 dilution), (viii) rabbit anti-mouse ALDH1L1 (Abcam, ab87117, 1:500), (ix) rabbit anti-mouse S100β (Abcam, Ab41548, 1:1000), (x) rabbit anti-mouse NEUN (Abcam, AB177487, 1:800); (xi) rabbit Neurofilament M (NFM) (EMD Millipore, AB1987, 1:1000). Fluorophore conjugated secondary donkey antibodies (Jackson Immuno-Research) raised against the various primary antibody species were applied for 2 hours. Tissue sections were stained for DAPI before being mounted on glass slides and coverslipped with Prolong™ Gold antifade mounting medium (Invitrogen).

Author Manuscript Author Manuscript Author Manuscript Author Manuscript

3. Results

3.1. Synthesis of non-ionic and cationic Met-based DCH

3.1.1. Design and synthesis of Met-based DCH precursors—Using previous DCH as models, new copolypeptides were designed as amphiphilic diblock copolymers with conformationally disordered, hydrophilic modified poly(L-methionine), **M**, segments and α-helical hydrophobic poly(L-leucine), **L**, segments to promote hydrogel self-assembly in aqueous media. We initially planned to prepare precursor copolypeptides of the general structure poly(L-methionine)$_{170}$-*b*-poly(L-leucine)$_n$, $\mathbf{M_{170}L_n}$, with *n* ranging from 15 to 40; where the **M** segments would then be oxidized or alkylated to give the DCH forming copolypeptides. However, an issue we observed when attempting to polymerize the long **M** segments required for DCH (> 150 residues) was that the resulting α-helical **M** chains strongly aggregate in the reaction solvent hindering the uniform addition of Leu NCA monomers for block copolymer preparation[49]. Consequently, initial attempts to oxidize and alkylate Met residues in $\mathbf{M_{170}L_n}$ resulted in samples unable to form hydrogels (*vide infra*). In order to address the problem of α-helical **M** chain aggregation, we relied on previous observations that aggregation of hydrophobic helical polypeptides in organic solvents can be diminished by statistical addition of comonomers to disrupt side-chain packing[24,49]. Hence, we incorporated small amounts of a non-ionic, low hydrophobicity comonomer, L-alanine (Ala), during **M** segment polymerization in order to disrupt packing of α-helical **M** chains and facilitate preparation of the desired diblock copolypeptide architectures[53].

Statistical copolymers of Ala NCA and Met NCA were prepared with target degrees of polymerization of *ca*. 100, where the Ala content was varied from 0 to 20 mol % (Scheme 1). The optimal Ala content was envisioned as the minimal amount required to disrupt polypeptide aggregation and allow efficient block copolypeptide synthesis. As expected, the $\mathbf{M_m}$ homopolymer containing no Ala formed an organogel in the reaction mixture due to chain aggregation. As the Ala content was increased, the poly(L-methionine-*stat*-L-alanine)$_m$, $\mathbf{MA_m}$, copolymers became more soluble in the reaction mixture, and eventually resulted in free-flowing viscous liquids at compositions 10 mol% Ala and above (Scheme 1). It is noteworthy that the incorporation of 10 mol% Ala did not adversely affect the ability to obtain controlled NCA polymerizations required for synthesis of well-defined block copolypeptides (Supplementary Figure 1). Also, incorporation of 10 or 18 mol% Ala in $\mathbf{MA_m}$ copolymers was found to have only minimal effect on the water solubility and disordered conformations of the corresponding oxidized poly(L-methionine sulfoxide-*stat*-L-alanine)$_m$, $\mathbf{M^OA_m}$, samples compared to $\mathbf{M^O}$ homopolymer (Supplementary Figure 2)[37,40]. Consequently, we selected **MA** copolymer segments containing 10 mol% Ala as optimized compositions for use in Met-based DCH.

Precursor diblock copolypeptides were then prepared containing **MA** segments *ca*. 170 residues long, followed by poly(L-leucine), **L**, segments of different length: poly(L-methionine$_{0.9}$-*stat*-L-alanine$_{0.1}$)$_{170}$-*b*-poly(L-leucine)$_n$, $\mathbf{(MA)_{170}L_n}$, with *n* ranging from *ca*. 10 to 40 (Scheme 2). Previous studies on DCH showed that small variations of **L** segment length have a much greater effect on DCH mechanical properties compared to small variations in the hydrophilic segment length[24,25]. All copolymers were isolated in high yield

Author Manuscript Author Manuscript Author Manuscript Author Manuscript

with compositions that closely matched expected values (Table 1). The **MA** segment length was chosen based on values known, from previous studies on amphiphilic DCH[24], to be sufficiently long to promote hydrogel formation. The **L** lengths were varied in order to study the role of hydrophobic composition on hydrogel formation and properties. Oxidation or methylation of these precursors using established methods[33,40] was envisioned to yield the corresponding amphiphilic $\mathbf{M^O}$ derivatives (i.e. DCH_{MO}) and $\mathbf{M^M}$ derivatives (i.e. DCH_{MM}), respectively, for evaluation as DCH (Scheme 2).

3.1.2. Synthesis of DCH_{MO} and DCH_{MM}—Complete and selective oxidation of $\mathbf{(MA)_{170}L_n}$ copolypeptides to the corresponding sulfoxide derivatives, $\mathbf{(M^OA)_{170}L_n}$ (i.e. DCH_{MO}), was accomplished using *tert*-butyl hydroperoxide (Table 1, Supplementary Information NMR spectra). We had previously used hydrogen peroxide for this purpose with shorter Met containing segments, but found that this reagent is not completely selective for MetO formation when longer, less soluble Met containing copolymers are oxidized. Small amounts of sulfone groups were observed to form with hydrogen peroxide (Supplementary Figure 3), which can adversely affect DCH_{MO} properties. As a different modification, selective methylation of $\mathbf{(MA)_{170}L_n}$ copolypeptides to the corresponding S-methyl sulfonium derivatives, $\mathbf{(M^MA)_{170}L_n}$ (i.e. DCH_{MM}), was accomplished using iodomethane, which gave the modified copolypeptides in excellent yields (Table 1, Supplementary Information NMR spectra). Both oxidation and methylation modifications of Met residues in these copolypeptides result in conversion of the fully hydrophobic $\mathbf{(MA)_{170}L_n}$ precursors into amphiphilic copolymers with potential to self-assemble in water and form DCH. Both modifications also convert α-helical **MA** segments in the copolymers into conformationally disordered $\mathbf{M^OA}$ and $\mathbf{M^MA}$ segments[30]. The modifications differ in that $\mathbf{M^OA}$ chains are non-ionic and hydrophilic, while $\mathbf{M^MA}$ chains are cationic and hydrophilic.

3.1.3. Synthesis of DCH_{MOK}—To study how introduction of charged groups into DCH_{MO} affects hydrogel properties we prepared a small series of samples where the Ala residues of DCH_{MO} were replaced with L-lysine, Lys, residues. The Lys residues were expected to assist controlled synthesis of long Met rich segments in a manner similar to Ala, as described above. In addition, these residues, when protonated, will introduce cationic charges into the hydrophilic segments of DCH_{MO}. Lys residues were introduced by copolymerization of different fractions of N-*tert*-butoxycarbonyl-L-Lysine NCA (Boc-Lys NCA), with Met NCA, followed by polymerization of the Leu block (Supplementary Scheme 1). Deprotection of the Lys residues using TFA, followed by selective oxidation of the Met residues gave the desired copolypeptides: poly(L-methionine sulfoxide$_x$-*stat*-L-lysine-HCl$_y$)$_{170}$-*b*-poly(L-leucine)$_{23}$, $\mathbf{(M^O_xK_y)_{170}L_{23}}$, with *x*:*y* = 0.90:0.10 (DCH_{MOK10}) and 0.85:0.15 (DCH_{MOK15}) (Supplementary Scheme 1 and Supplementary Table 2). Copolymerization, subsequent deprotection and oxidation proceeded without issues, showing that another comonomer beside Ala can be used to prepare well-defined copolypeptides containing long Met rich segments. The introduction of charged Lys residues into DCH_{MOK} was expected to affect both physical and biological properties of these materials.

Author Manuscript Author Manuscript Author Manuscript Author Manuscript

3.2. Formulation and properties of Met-based DCH

3.2.1. Preparation and rheological properties of DCH_{MO} and DCH_{MM}—For initial evaluation, all DCH_{MO} and DCH_{MM} samples, as well as Ala lacking $\mathbf{(M^{O})_{170}L_{23}}$ and $\mathbf{(M^{M})_{170}L_{24}}$ control samples, were separately mixed with deionized (DI) water at concentrations ranging from 1.0 to 9.0 wt% (Table 2). These samples were briefly agitated and then let stand for 24h, whereupon they were visually examined (Supplementary Figure 4). At 1.0 wt%, all samples formed free-flowing, transparent fluids. As concentrations were increased, all DCH_{MO} and DCH_{MM} samples were observed to form hydrogels, except for those with the shortest **L** segments, $\mathbf{(M^{O}A)_{170}L_{12}}$ and $\mathbf{(M^{M}A)_{170}L_{12}}$, which were both transparent fluids up to 9.0 wt%. DCH_{MM} samples were generally found to form hydrogels at lower concentrations compared to analogous DCH_{MO} samples of similar composition. For all DCH_{MO} and DCH_{MM} samples with $\mathbf{L_{17}}$ segments or longer, hydrogel formation improved with both **L** segment length and sample concentration. However, in samples with longer **L** segment lengths and at higher concentrations, copolypeptide precipitation was also observed in these hydrogels. Hydrogel opacity was generally more pronounced in the DCH_{MM} samples relative to DCH_{MO} samples (Supplementary Figure 4). It is noteworthy that the Ala lacking $\mathbf{(M^{O})_{170}L_{23}}$ and $\mathbf{(M^{M})_{170}L_{24}}$ samples were unable to form hydrogels (Supplementary Figure 5), except for $\mathbf{(M^{M})_{170}L_{24}}$ that formed an opaque hydrogel at 9 wt%. These results confirm the importance of copolymerization of Ala residues into the Met segments for DCH formation.

To quantify hydrogel properties, oscillatory rheology studies were conducted on select DCH_{MO} and DCH_{MM} samples. For DCH_{MO} samples at 5.0 wt% in DI water, hydrogel stiffness (G') was found to increase with **L** segment length up to $\mathbf{L_{28}}$, yet precipitation in samples with longer **L** segments reversed this trend (Figure 1A). Due to its desirable combination of hydrogel stiffness and minimal turbidity, $\mathbf{(M^{O}A)_{170}L_{28}}$ was chosen as an optimized DCH_{MO} composition for further mechanical properties study. Preparation of DCH_{MO} using different concentrations of $\mathbf{(M^{O}A)_{170}L_{28}}$ in DI water was found to be a convenient means to adjust hydrogel stiffness (Figure 1B). All samples formed clear elastic hydrogels ($G' \gg G''$ over a range of frequency, Figure 1C), and their stiffness was found to increase with higher copolypeptide concentrations. The lack of visible aggregates in these samples suggests that polymer chains were able to assemble into the desired structures even at high concentrations. The self-healing properties of DCH_{MO} after mechanical breakdown were studied by repeatedly subjecting a 5.0 wt% $\mathbf{(M^{O}A)_{170}L_{28}}$ sample in DI water to high amplitude oscillatory strain, and then monitoring the recovery of elasticity over time by measuring G' at a much smaller strain amplitude (Figure 1D). The periods of high strain resulted in G' dropping by two orders of magnitude to below the level of G'', indicating the sample had become a viscous liquid. Upon switching to low strain, the sample self-healed to recover its elastic properties, with most of the original gel stiffness regained within the brief period (*ca.* 10 s) needed to switch between strain amplitudes.

For DCH_{MM} samples at 5.0 wt% in DI water, hydrogel stiffness (G') was also found to increase with **L** segment length up to $\mathbf{L_{33}}$, and then leveled off as sample precipitation occurred with longer **L** segments (Figure 2A). The increased hydrophilicity of the charged $\mathbf{M^{M}}$ segments compared to non-ionic $\mathbf{M^{O}}$ segments may be responsible for the significantly

Author Manuscript Author Manuscript Author Manuscript Author Manuscript

greater stiffness of these samples compared to DCH_{MO}. For reasons similar to those stated for DCH_{MO}, $\mathbf{(M^{M}A)_{170}L_{27}}$ was chosen as an optimized DCH_{MM} composition for further mechanical properties study. Preparation of this DCH_{MM} at different concentrations in DI water was similarly found to conveniently adjust hydrogel stiffness (Figure 2B). All samples formed elastic hydrogels ($G' \gg G''$ over a range of frequency, Figure 2C) with stiffness that increased with higher copolypeptide concentrations. However, in contrast to DCH_{MO} of similar composition, visible aggregates were observed at sample concentrations greater than 5.0 wt%. The 5.0 wt% $\mathbf{(M^{M}A)_{170}L_{27}}$ sample in DI water was also able to exhibit shear thinning and self-healing properties comparable to results observed above with DCH_{MO} (Figure 2D).

3.2.2. Effects of ionic media on DCH_{MO} and DCH_{MM}—Select DCH_{MO} and DCH_{MM} samples ($\mathbf{(M^{O}A)_{170}L_{24}}$ and $\mathbf{(M^{M}A)_{170}L_{23}}$) were also prepared in different aqueous media (Figure 3). We used these samples, containing $\mathbf{L_{23/24}}$ hydrophobic segments, since their mechanical properties were closest to those of hydrogel formulations we have found to be useful for CNS applications. Samples were prepared at 5 wt% in either DI water, 1× PBS buffer, or DMEM cell culture medium, and their rheological behavior studied. Mechanical properties of the non-ionic DCH_{MO} formulations were minimally affected by the ions present in media (Figure 3A, B), allowing for predictable mechanical behavior under different solution conditions. Conversely, mechanical properties of the cationic DCH_{MM} formulations were strongly affected by the ions present in media (Figure 3C,D), with hydrogel stiffness (G') decreasing significantly in the presence of ions compared to DI water. Notably, different media (PBS and DMEM) had similar effects on DCH_{MM} properties, and the DCH_{MM} in these media remained hydrogels with stiffness comparable to analogous DCH_{MO} formulations. Another difference observed between DCH_{MO} and DCH_{MM} formulations was their breakdown at elevated percent strain. The DCH_{MM} formulations were found to be more brittle than analogous DCH_{MO} formulations, especially in ionic media, where the DCH_{MM} samples were observed to breakdown at relatively low percent strain (Figure 3B, D). As shown above, at very high percent strains (*ca.* > 1000%), both DCH_{MO} and DCH_{MM} will break down into liquids.

3.2.3. Rheological properties of DCH_{MOK}—The Lys containing samples DCH_{MOK10} and DCH_{MOK15} were mixed with DI water or 1× PBS to give concentrations of 5.0 wt% and were found to form hydrogels in both media after standing for 24h. In DI water, DCH_{MOK10} and DCH_{MOK15} formed hydrogels with stiffness (G') intermediate between those of DCH_{MO} and DCH_{MM} at similar compositions (Figure 4, Supplementary Figure 6). Hydrogel stiffness was found to increase with increased ionic residue content in the DCH, where even 15 mol% charged residues in the hydrophilic DCH segments was sufficient to result in hydrogel stiffness comparable to that obtained with the fully charged segments in DCH_{MM}. Increased charged residue content also significantly impacted hydrogel salt stability, where DCH_{MOK15} was found to weaken significantly in PBS, similar to DCH_{MM}. DCH_{MOK10} behaved more like DCH_{MO} in PBS, where hydrogel stiffness was even found to increase in ionic media. From these observations, it can be seen that small variations in charged residue content in DCH_{MOK} can result in substantial effects on both hydrogel stiffness and salt stability.

Author Manuscript Author Manuscript Author Manuscript Author Manuscript

3.3. NSPC viability in Met-based DCH

For CNS cell transplantation a cell compatible biomaterial vehicle that promotes negligible cytotoxicity is required. To test the cell viability of Met-based DCH materials we derived a passagable, adherent neural stem/progenitor cell (NSPC) line from mouse embryonic stem cells (ESC) using previously validated and published protocols (Supplementary Figure 7A)[55–57]. The use of an ESC derived NSPC line overcame many of the quality and reproducibility limitations associated with using primary cells harvested from fetal or post-natal tissue that we have employed in our previous studies[28,53]. Before encapsulating cells in DCH formulations we confirmed NSPC derivation by qPCR and immunohistochemical analysis (Supplementary Figure 7B). The adherent NSPC line showed characteristic increased expression of canonical neural stem cell genes (*Nestin, Sox2, Sox9, Olig2*) as well as a de-enrichment of classic ES identifiers *Nanog* and *Oct4* (Supplementary Figure 7B). Immunocytochemical staining further confirmed robust protein expression of the same canonical neural stem cell markers in our NSPC line (Supplementary Figure 7C, D). The NSPC used in this study contain a hemagglutinin (HA) tag on ribosomal protein L22, a component of the 60S ribosomal subunit (referred to here as Ribotag). This Ribotag can be used as an *in vivo* reporter to distinguish transplanted NSPCs from host cells by immunohistochemistry as well as allowing for cell specific translating mRNA extraction from whole tissue[54]. We confirmed 100% expression of the HA Ribotag in every cell in the NSPC line by immunocytochemistry (Supplementary Figure 7E). The NSPC line showed negligible expression of the pan astrocyte marker GFAP and pan neuronal marker TUJ-1 by immunohistochemical staining under regular culture conditions. However, NSPC showed a competency to differentiate into these two cell types upon exposure to fetal bovine serum (FBS) enriched media consistent with previous characterization of similar NSPC lines (Supplementary Figure $7E_1$)[56,58]. Before and after neuronal or astrocyte differentiation the cells maintained robust HA expression that filled the entire cell cytoplasm (Supplementary Figure $7E_2$).

To evaluate the relative cell compatibility of the various Met-based DCH vehicles we encapsulated NSPC within DCH_{MO}, DCH_{MM}, DCH_{MOK10} and DCH_{MOK15} formulations and incubated the cell-hydrogel construct on top of beds of cell media enriched agarose gels for 24 hours. Specific copolypeptide compositions used in these and all subsequent biological studies were $\mathbf{(M^{O}A)_{170}L_{24}}$, $\mathbf{(M^{M}A)_{170}L_{23}}$, $\mathbf{(M^{O}_{0.90}K_{0.10})_{170}L_{23}}$, and $\mathbf{(M^{O}_{0.85}K_{0.15})_{170}L_{23}}$. Cell viability was determined by analyzing the distribution of live and dead cells using calcein AM and ethidium homodimer-1 staining. The non-ionic DCH_{MO} showed excellent NSPC viability for all formulations tested from 2 to 5 wt% copolypeptide. The negligible cytotoxicity for DCH_{MO} over the 24 hour period was equivalent to that observed for the positive control of cells alone in media (Figure 5A, B, D). By contrast DCH_{MM} formulations containing positively charged sulfonium functional groups demonstrated substantial NSPC cytotoxicity which was equivalent to the cell death observed for DCH_K, another cationic copolypeptide hydrogel we have shown previously to be cytotoxic towards various suspended cells[28,53] (Figure 5A, D). The Lys containing hydrogels DCH_{MOK10} and DCH_{MOK15} showed reduced NSPC viability compared to DCH_{MO} with cytotoxicity increasing in a Lys concentration dependent manner. Specifically, DCH_{MOK10} showed 80.7% NSPC viability while DCH_{MOK15} demonstrated comparable cytotoxicity to

Author Manuscript Author Manuscript Author Manuscript Author Manuscript

that observed for DCH_{MM} and DCH_K suggesting this to be the minimum Lys content required within DCH polypeptides for complete lysis of suspended cells. (Figure 5C).

3.4. NSPC adhesion to Met-based DCH

Cell-biomaterial interactions may influence NSPC transplant outcomes[59]. Since $\mathbf{M^O}$ polypeptides have previously been demonstrated to be non-fouling, bioinert substrates for cells *in vitro*[41], we sought to evaluate NSPC interactions with Met-based DCH. To achieve this, we assessed the ability of NSPC to adhere to substrates coated with the various Met-based DCH and compared and normalized them to a standard cell adhesion promoting biomolecule, gelatin, which is used widely across adherent *in vitro* assays. The use of 70% ethanol solutions of Met-based DCH ensured robust copolypeptide coating to either hydrophobic siliconized glass slides or hydrophobic untreated polystyrene. Calcein AM staining after vigorous washing to remove non-adhered cells was used to quantify the amount of viable adhered cells to each substrate. At 24 hours after seeding NSPC in FBS enriched media, DCH_{MO} showed negligible NSPC adhesion (0.23% of the gelatin coated substrate cell number) and instead led to significant cell aggregation resulting in large clumps of cells that were hundreds of μm in diameter (Figure 6A, B, Supplementary Figure 8). The minimal cell adhesion was equivalent to that achieved for the amphiphilic PEG based negative control. By contrast, the DCH_{MM} with 63.2% adhered cells was comparable to that seen for the positively charged Lys based DCH_K (74.3%) with cells displaying a characteristic adherent, flattened morphology by brightfield microscopy (Figure 6A, B). Introduction of cationic charge within DCH_{MO} via replacement of Ala with Lys residues (i.e. DCH_{MOK10}, DCH_{MOK15}) increased the cellular interactions with the copolypeptide chains and consequently increased cell adhesion to coated substrates. Cell adhesion increased in a Lys concentration dependent manner with DCH_{MOK10} maintaining 30.3% cell adhesion while DCH_{MOK15} showing 76.7% cell adhesion. Cells on surfaces of DCH_{MOK10} adhered as small multi-cellular aggregates that were smaller in size than those seen in the DCH_{MO} samples with some flattened adherent cells visible at the margins of the aggregate (Figure 6B). The extent of cell adhesion for DCH_{MOK15} was comparable to DCH_K and DCH_{MM} suggesting that the charge distribution on the DCH_{MOK15} represented the minimum amount of net charge needed along DCH copolypeptide chains to promote significant interaction with NSPC. Interestingly, the cell adhesion data was inversely related to the observed cell viability results articulated above when NSPC were suspended within the same DCH formulation. These data suggest that non-specific cationic charge based cell interactions can robustly encourage NSPC to adhere to a constrained two dimensional substrate with negligible cytotoxicity. However, when the cells are immersed within DCH containing the same hydrophilic chains, the strength and concentration of these polymer-cell interactions, which are less constrained in space and undergo dynamic movement around the encapsulated NSPC, results in cell membrane disruption and/or lysis causing cell death.

3.5. NSPC differentiation with Met Based DCH

Physical interactions of stem cells with the extracellular matrix environment are principal determinants of cell fate decision making[60]. Similarly, NSPC differentiation outcomes upon transplantation in the CNS are also influenced by their interactions with biomaterial carriers[61], as well as with host tissue elements. To understand how cellular interactions with

Author Manuscript Author Manuscript Author Manuscript Author Manuscript

the Met-based DCH influence NSPC cell fate outcomes we devised an assay to evaluate NSPC differentiation on DCH coated substrates. Towards replicating the environment the transplanted NSPC would experience *in vivo* within the context of CNS injury we cultured NSPC in media containing 10% FBS along with standard NSPC supplements (EGF, FGF and B27). NPSC differentiation was evaluated on substrates of DCH_{MO}, DCH_{MM} or gelatin for 48 hours. After 48 hours in this serum rich environment the cells were transferred to unsupplemented conditions on gelatin substrates to evaluate the spontaneous differentiation of these cells following FBS treatment (Figure 7A). NSPC differentiation was significantly influenced by the chemical properties of the substrate (Figure 7B, C, Supplementary Figure 9). NSPC cultured on gelatin during the 48 hours of FBS exposure exhibited a significantly increased density of GFAP positive cells normalized to HA positive cell signal (a measure of total surface area occupied by cells on the substrate) compared to the DCH_{MO} and DCH_{MM} coated substrates. By contrast, a predominately neuronal differentiation phenotype (as measured by TUJ-1 positive cell density) was observed on the DCH_{MM} coated substrate. The DCH_{MO} coated surface, unlike the two cell adhesive substrates, exhibited no clear dominant differentiated cell type and showed an overall reduced extent of total cell differentiation that was approximately half of that observed on the gelatin surface (Figure 7C). To understand why the DCH_{MM} coated substrate showed a preferred neuronal differentiation profile compared to gelatin, we compared NSPC phenotypes immediately after FBS exposure by immunocytochemistry (Figure 7D). While gelatin coated substrates showed a dense field of GFAP and TUJ-1 positive cells at the conclusion of FBS treatment, cells on DCH_{MM} expressed exclusively TUJ-1 that was distributed diffusely throughout the cell cytoplasm rather than being organized in ordered, filamentous cytoskeletal structures that is characteristic of cultured neurons.

NSPC cultured on DCH_{MM} were also less dense in number and exhibited a larger and more flattened cell morphology with extensive filopodia projections that varied in shape and size between different cells throughout the surface. The relative strength of the cell interactions with the DCH_{MM} substrate was further characterized by assessing the number of cells that remained on the surface following a trypsinization procedure (Figure 7E). While complete cell removal off of the gelatin surface was achieved following trypsinization, approximately 12% viable cells remained on DCH_{MM} following the same procedure. This residual adhered cell number is likely an under estimate of the total remaining cells after trypsinization as this procedure can be considerably cytotoxic to persistently adhered cells and our outcome measure (Calcien AM staining) only identified live, viable cells. Regardless of the exact percentage of remaining cells, the relatively high number of residual cells comparatively to the gelatin substrate coupled with the flattened, irregular cell morphology suggests a particularly strong cell interaction with DCH_{MM}. Additionally, qPCR was performed on cells collected at the end of the 48 hour FBS treatment to evaluate the effect of surface properties on the gene expression of neural stem cell and neural cell type specific markers (Figure 7F). In line with the immunocytochemistry data, cells cultured on DCH_{MO} showed a more preserved progenitor-like gene profile upon FBS exposure with canonical neural stem cell genes *Nestin* and *Sox9* being less down regulated in this group compared to cells cultured on the adhesive substrates. Interestingly, *GFAP* gene expression was highest for DCH_{MO} over all other groups, while *GFAP* was also significantly expressed by cells on

Author Manuscript Author Manuscript Author Manuscript Author Manuscript

DCH_{MM}. The mismatch between *GFAP* mRNA abundance and protein expression levels measured by immunocytochemistry across the different treatments suggests that the physical substrate and how cells interact with it may influence important cellular functions such as mRNA post transcriptional modifications, protein synthesis and cytoskeletal protein assembly. Overall, these data suggest that the non-adhesive DCH_{MO} preserves the multipotency of NSPC in serum rich environments compared to adhesive materials. This unique biological property of DCH_{MO} may prove to be useful for ensuring robust survival and integration of transplanted NSPC within CNS injury microenvironments.

3.6. *In vivo* NSPC transplantation using Met-based DCH

To evaluate the utility of Met-based DCH as biomaterial carriers for CNS transplantation we first injected empty DCH_{MO} into the uninjured mouse striatum and compared the induced foreign body response to a saline control. DCH_{MO} alone caused minimal host CNS tissue disruption. Specifically, the proximal neuronal survival as well as the extent and magnitude of the reactive astroglial response for the DCH_{MO} was comparable to that of the saline injection (Supplementary Figure 10). Next, we transplanted NSPC encapsulated within DCH_{MO} into the uninjured mouse striatum. The NSPC suspended uniformly within DCH_{MO} and did not sediment or aggregate throughout the entire duration of both the glass pipette loading and the slow controlled injection procedure, which was similar to that seen for our previously studied formulations[28]. Gene profiling of NSPC suspended within DCH_{MO} recovered from the un-injected fraction of biomaterial at 6 hours after initial cell loading showed negligible change in gene expression of canonical neural stem cell genes for the injected cells compared to the *in vitro* cultured NSPC line (Supplementary Figure 11). At 4 weeks after transplantation NSPC injected brains were analyzed by immunohistochemistry (Figure 8). Injected NSPC loaded in DCH_{MO} formed an obvious and focal deposit within host tissue that persisted over the 4 week observation period. Transplanted cells as well as any potential progeny were readily identified by HA immunohistochemical staining. Transplanted cells were observed within the hydrogel as multicellular neurosphere aggregates that had adhered to the margins of the hydrogel deposit and subsequently integrated with host tissue (Figure 8). Within host tissue, transplanted cells were constrained within a tissue volume region that was within several hundred μm of the border of the hydrogel deposit (Figure 8). Thus the use of the DCH_{MO} vehicle prevented long distance migration of transplanted cells away from the injection zone to other brain regions. Essentially all transplanted cells expressed GFAP robustly by 4 weeks but also maintained widespread expression of the canonical neural stem cell markers SOX9 (Figure 8A, B), SOX2 (Figure 8C) and NESTIN (Figure 8D) characteristic of an immature astroglial phenotype[58]. This extensive GFAP expression represented an upregulation of this astroglial marker compared with the NSPC at the time of transplantation. Grafted cells were uniformly negative for the neuronal marker TUJ-1 (Supplementary Figure 12). By four weeks the numerous transplanted cells that had integrated into the adjacent host tissue had adopted distinct, individual cellular domains reminiscent of normal host astroglial cells[62] (Figure 8B).

Immunohistochemical evaluation revealed that host neurons (Figure 9) and host astrocytes (Figure 10) persisted with normal density and viability at the edge of the NSPC graft

Author Manuscript Author Manuscript Author Manuscript Author Manuscript

margin. HA positive transplanted cells with their GFAP positive cellular processes integrated into fields of, and interacted directly with, host NEUN positive neurons (Figure 9A, B). In addition to direct interactions with neuronal somas, grafted cells showed a capacity to act as cellular substrates to attract and support the growth of host axons. Specifically, using Neurofilament M (NFM) to label host axons, we observed that the transplanted NSPC functioned as cellular bridges permitting regrowth of meandering host axons into the DCH_{MO} deposit site (Figure 9C, D). Such a function is consistent with the role host immature astroglia play during CNS development to support and guide axon growth[63] and may be important for promoting regeneration of damaged axons in the context of CNS injury[26,28,64]. While the HA positive transplanted cells expressed high levels of GFAP, they did not express the more mature astrocyte marker ALDH1L1 (Figure 10A, C), further supporting the notion that these cells had persisted as immature astroglial cells throughout the 4 weeks of residence in the uninjured CNS[56,65]. Some HA positive cells expressed an alternative but less mature astrocyte marker, S100β, suggesting the transplanted cells may be progressing through astrocyte maturation. However, S100β expression was not widespread among all transplanted cells (Figure 10B). Despite their immature phenotype, grafted cells were observed to interact directly, and intermingle, with host astrocytes (Figure 10C). Host astrocytes were also observed to migrate into the persistent DCH_{MO} deposit site that contained a high density of grafted cells (Figure 10A, B), creating a fluid transition of intermingled host and grafted astroglia at the margins of the graft deposit. Furthermore, at the margins of the DCH_{MO} deposit there was no evidence of host astrocyte scarring or walling off of the NSPC-hydrogel implant, while host astrocytes in close proximity of the DCH deposit margin were only mildly reactive and maintained discrete individual cellular domains. Overall, these findings suggest that NSPC transplanted in DCH_{MO} can provide cells that integrate well with receptive host neural tissue and serve supportive functions that may be useful for neural repair.

4. Discussion

In this study, we developed a novel biomaterial platform focused on the post-polymerization modification of Met-based copolypeptides. These new materials show diverse and tunable physiochemical and biological properties with some formulations demonstrating utility as vehicles for aiding the *in vivo* transplantation of NSPC in the CNS. Our findings have implications at several levels, including (i) the technical development of non-ionic biomaterial vehicles for NSPC delivery; (ii) the influence of Met-based DCH on NSPC survival and differentiation; and (iii) the potential of Met-based DCH for NSPC transplantation into injured CNS.

4.1. Technical considerations regarding development of non-ionic, Met-based DCH

We have shown previously that ionic DCH such as DCH_K are useful vehicles for delivery of both small molecule and protein biologically active agents into mouse CNS tissues *in vivo*. In particular, the modular design of DCH permits fine tuning of their physical characteristics for specific applications, and their synthetic nature allows for scalable synthesis and reproducible formulation. An initial effort to prepare non-ionic DCH for encapsulation of cells *in vitro* and their grafting into tissues *in vivo* used synthetic methods relying on

Author Manuscript Author Manuscript Author Manuscript Author Manuscript

unnatural amino acid components that limited scalability and prohibited incorporation of functionality into these DCH[28]. To correct these limitations, we envisioned Met-based DCH as a versatile platform of precursor copolypeptides that could be selectively modified at Met residues using a variety of efficient procedures to give DCH with different physical and biological properties. Initial targets for evaluation were non-ionic DCH_{MO} and a model cationic derivative, DCH_{MM}.

Aggregation of **M** polymers during synthesis was an initial hurdle that was overcome by judicious addition of comonomers, i.e. Ala and Lys, which were found to disrupt helical side-chain packing of **M** segments and thus enabling controlled synthesis of Met DCH precursors. The need to incorporate comonomers in the **M** segments was found to be advantageous, as they can provide additional means to fine tune DCH properties. Ala residues were found to act as inert diluents that imparted no adverse effects on the properties of the modified **M** segments. Incorporation of Lys residues was found to be a useful means to introduce controllable quantities of charged residues into $\mathbf{M^O}$ segments. Another potentially useful feature of these Met DCH precursors is that some of the Met or Lys residues can also serve as sites for selective conjugation of bioactive molecules or fluorescent probes for added functionality[30].

Straightforward modification of Met DCH precursors using literature methods gave non-ionic DCH_{MO} and cationic DCH_{MM} with near quantitative levels of functionalization in excellent yields. Both DCH_{MO} and DCH_{MM} of different compositions formed hydrogels over a range of concentrations in DI water. At equivalent compositions and concentrations, DCH_{MO} formed inherently weaker hydrogels compared to DCH_{MM}, which is likely due to the greater water solubility, and electrostatic repulsions in the cationic $\mathbf{M^MA}$ segments compared to non-ionic $\mathbf{M^OA}$ segments. However, DCH_{MO} were found to be more ductile and stable to ionic media compared to DCH_{MM}, such that hydrogel stiffness of comparable samples was very similar in ionic media. This finding is important since both of these hydrogels will be used primarily in ionic media for all biological studies. Overall, both DCH_{MO} and DCH_{MM} were found to possess desirable physical properties for evaluation as vehicles in CNS applications, including injectability and tunable stiffness and surface functionality. We were particularly interested to study how variation of charge content in DCH_{MO}, DCH_{MOK} and DCH_{MM} affects how these hydrogels interact with cells.

4.2. The influence of Met-based DCH on NSPC survival and differentiation

Cues from the extracellular environment both within *in vitro* culture conditions and neural tissue niches *in vivo* shape the differentiation decision making of NSPC. Detailed experimental information pertaining to the relative importance of various stimuli, including the physiochemical properties of biomaterial carriers, on NSPC differentiation is beginning to emerge[22]. In particular, properties such as mechanical stiffness and biomaterial degradability have been extensively studied[63]. Here, by leveraging the physiochemical tunablity of Met-based DCH through various post-polymerization modifications, we characterized and optimized the effect of biomaterial surface chemistry on NSPC differentiation. DCH_{MO} by virtue of its non-fouling sulfoxide functionality showed a remarkable preservation of neural stemness in a serum rich *in vitro* environment compared

Author Manuscript Author Manuscript Author Manuscript Author Manuscript

to adhesive substrates DCH_{MM} and Gelatin. To improve survival of NSPC upon transplantation in traumatic CNS lesions a biomaterial carrier capable of keeping the cells in a more robust immature state for longer upon grafting would be advantageous.

In addition to the development of a novel hydrogel we also describe here for the first time the derivation of a Ribotag NSPC line. Ribotag is a cell specific mRNA isolation technique from whole tissue that has gained in popularity over the past several years[26,54,66]. This paper describes and validates the derivation of the Ribotag NSPC line from transgenic ESC and demonstrates the preservation of detectable HA positive ribosomes within cells throughout the various stages of NSPC development and differentiation. While not explored here, the goal for the use of these cells in future experiments is to perform *in vivo* transplant cell specific genetic evaluation in the context of CNS injury. This paper represents a first step towards this goal by demonstrating the ability to: (i) detect HA positive NSPC and their progeny by immunohistochemistry *in vitro* and in whole tissue after grafting *in vivo*, as well as (ii) characterize the robustness of Ribotag mRNA expression within cells at various stages of development both *in vitro* and *in vivo* such that it could be used as a housekeeping gene to normalize gene expression data. Furthermore, the robust and persistent expression of Ribotag by NSPC and their progeny *in vivo*, provides a means of selective isolation of transcribed mRNA specifically from grafted cells for analysis of changes in their transcriptional profiles at different times after transplantation and under different grafting conditions. Given the interesting findings pertaining to the variation in NSPC differentiation *in vitro* as a function of material surface properties and exposure to different morphogens, future experiments using these cells can be directed towards obtaining a detailed understanding of the effect of hydrogel carrier properties and effects of co-delivery of regulatory molecules on NSPC differentiation *in vivo*.

4.3. The potential of Met-based DCH for NSPC transplantation into CNS injury

In the context of CNS insults such as spinal cord injury, traumatic brain injury or stroke damage of neural tissue results in a biologically conserved wound healing response that leads to the formation of non-neural tissue (NNT) lesions[67,68]. NNT lesions hinder endogenous recovery/regeneration of damaged neural circuitry as this tissue is permanently devoid of functioning neurons and glia. Grafting of NSPC has emerged as a potential therapy for CNS injury by repopulating NNT lesions with a neural cell milieu that can provide both the trophic support and physical substrates necessary to aid the axon regeneration required to reestablish functioning circuits[68]. In this study we showed that transplanted NSPC, in the absence of differentiation directing morphogens, adopt immature astroglial phenotypes at 4 weeks that were capable of interacting with host astrocytes and neurons as well as acting as a cellular substrate for regrowing axons locally in the vicinity of the injected hydrogel. DCH_{MO} aided in keeping transplanted cells local to the injection site but still permitted comprehensive integration with host neural tissue. Transplanted cells adopted an immature astroglial cell state (as demonstrated by robust GFAP, SOX2, SOX9 and NESTIN expression) and no transplanted cells expressed the pan-neuronal maker TUJ-1 or the mature astrocyte marker ALDH1L1. These results indicate that, in the absence of co-delivery of differentiation directing morphogens, these cells do not undergo any significant spontaneous differentiation and maturation *in vivo*, at least up to 4 weeks. We have

Author Manuscript Author Manuscript Author Manuscript Author Manuscript

previously shown that DCH vehicles can be used to controllably delivery a variety of small molecule and protein based drugs to the CNS[26]. Therefore, future studies will explore using DCH_{MO} to co-deliver both NSPC and specific bioactive morphogens to facilitate specific *in vivo* directed differentiation and maturation of transplanted cells.

5. Conclusion

In this study we developed a new Met-based DCH platform that overcame several synthetic limitations associated with previous formulations and demonstrated tunable physiochemical and biological properties. Met-based DCH also offer considerable flexibility in terms of converting Met residues to different functional derivatives, as well as the ability to incorporate different amino acid comonomers into their hydrophilic segments. The non-ionic DCH_{MO} formulations were found to be advantageous for cell transplantation applications since they possess: (i) favorable cytocompatibility, (ii) cell non-fouling properties, and (iii) an ability to better persevere NSPC stemness in serum rich environments compared to adhesive substrates. DCH_{MO} facilitated local injection and retention of NSPC and its progeny in the uninjured mouse CNS. In the absence of added morphogens, transplanted cells maintained an immature astroglial phenotype at 4 weeks that favorably interacted with host neural tissue and acted as a cellular substrate to aid regeneration of host-derived damaged or sprouted axons. These findings suggest that DCH_{MO} is a suitable hydrogel carrier for neural stem cell transplantation applications and warrants further investigation as a therapeutic tool in CNS injury studies.

Supplementary Material

Refer to Web version on PubMed Central for supplementary material.

Acknowledgments

We thank the Microscopy Core Resource of the UCLA Broad Stem Cell Research Center-CIRM Laboratory as well as the lab of Tatiana Segura at UCLA for generously providing access to equipment for the rheological experiments. This work was supported by the Dr. Miriam and Sheldon G. Adelson Medical Foundation (M.V.S. and T.J.D.), the US National Institutes of Health (NS084030 to M.V.S. and AI112016 to T.J.D.), and the Craig H. Neilsen Foundation (381357 to T.M.O.).

References

1O'Shea TM. Smart Materials for Tissue Engineering: Applications Wang Qun, editorRoyal Society of Chemistry; 2017

2Mothe AJ, Tator CH. Advances in stem cell therapy for spinal cord injury. The Journal of Clinical Investigation. 2012; 122:3824–3834. [PubMed: 23114605]

3Vadivelu S, et al. NG2+ Progenitors Derived From Embryonic Stem Cells Penetrate Glial Scar and Promote Axonal Outgrowth Into White Matter After Spinal Cord Injury. Stem Cells Translational Medicine. 2015; 4:401–411. [PubMed: 25713464]

4Cao Q-L, et al. Pluripotent Stem Cells Engrafted into the Normal or Lesioned Adult Rat Spinal Cord Are Restricted to a Glial Lineage. Experimental Neurology. 2001; 167:48–58. [PubMed: 11161592]

5Wu S, et al. Migration, integration, and differentiation of hippocampus-derived neurosphere cells after transplantation into injured rat spinal cord. Neuroscience Letters. 2001; 312:173–176. [PubMed: 11602338]

Author Manuscript Author Manuscript Author Manuscript Author Manuscript

6Lu P, et al. Long-Distance Growth and Connectivity of Neural Stem Cells after Severe Spinal Cord Injury. Cell. 2012; 150:1264–1273. [PubMed: 22980985]

7Nori S, et al. Grafted human-induced pluripotent stem-cell derived neurospheres promote motor functional recovery after spinal cord injury in mice. Proceedings of the National Academy of Sciences. 2011; 108:16825–16830.

8Falkner S, et al. Transplanted embryonic neurons integrate into adult neocortical circuits. Nature. 2016; 539:248. [PubMed: 27783592]

9Hallett Penelope J, , et al. Successful Function of Autologous iPSC-Derived Dopamine Neurons following Transplantation in a Non-Human Primate Model of Parkinson's Disease. Cell Stem Cell. 2015; 16:269–274. [PubMed: 25732245]

10Assinck P, Duncan GJ, Hilton BJ, Plemel JR, Tetzlaff W. Cell transplantation therapy for spinal cord injury. Nature Neuroscience. 2017; 20:637. [PubMed: 28440805]

11Nishimura S, et al. Time-dependent changes in the microenvironment of injured spinal cord affects the therapeutic potential of neural stem cell transplantation for spinal cord injury. Molecular Brain. 2013; 6

12Piltti KM, Salazar DL, Uchida N, Cummings BJ, Anderson AJ. Safety of epicenter versus intact parenchyma as a transplantation site for human neural stem cells for spinal cord injury therapy. Stem Cells Transl Med. 2013; 2:204–216. [PubMed: 23413374]

13Steward O, Sharp KG, Yee KM, Hatch MN, Bonner JF. Characterization of Ectopic Colonies That Form in Widespread Areas of the Nervous System with Neural Stem Cell Transplants into the Site of a Severe Spinal Cord Injury. The Journal of Neuroscience. 2014; 34:14013–14021. [PubMed: 25319698]

14Tuszynski Mark H, , et al. Neural Stem Cell Dissemination after Grafting to CNS Injury Sites. Cell. 2014; 156:388–389. [PubMed: 24485445]

15Kadoya K, et al. Spinal cord reconstitution with homologous neural grafts enables robust corticospinal regeneration. Nature Medicine. 2016; 22:479–487.

16Lu P, et al. Long-Distance Axonal Growth from Human Induced Pluripotent Stem Cells after Spinal Cord Injury. Neuron. 2014; 83:789–796. [PubMed: 25123310]

17McCreedy DA, et al. Survival, differentiation, and migration of high-purity mouse embryonic stem cell-derived progenitor motor neurons in fibrin scaffolds after sub-acute spinal cord injury. Biomaterials Science. 2014; 2:1672–1682. [PubMed: 25346848]

18Hoare TR, Kohane DS. Hydrogels in drug delivery: Progress and challenges. Polymer. 2008; 49:1993–2007.

19Murphy WL, McDevitt TC, Engler AJ. Materials as stem cell regulators. Nature Materials. 2014; 13:547. [PubMed: 24845994]

20Mothe AJ, Tam RY, Zahir T, Tator CH, Shoichet MS. Repair of the injured spinal cord by transplantation of neural stem cells in a hyaluronan-based hydrogel. Biomaterials. 2013; 34:3775–3783. [PubMed: 23465486]

21Ballios BG, et al. A Hyaluronan-Based Injectable Hydrogel Improves the Survival and Integration of Stem Cell Progeny following Transplantation. Stem Cell Reports. 2015; 4:1031–1045. [PubMed: 25981414]

22Madl CM, et al. Maintenance of neural progenitor cell stemness in 3D hydrogels requires matrix remodelling. Nature Materials. 2017; 16:1233. [PubMed: 29115291]

23Altunbas A, Pochan DJ. Peptide-based and polypeptide-based hydrogels for drug delivery and tissue engineering. Topics in current chemistry. 2012; 310:135–167. [PubMed: 21809190]

24Deming TJ. Polypeptide hydrogels via a unique assembly mechanism. Soft Matter. 2005; 1:28–35.

25Nowak AP, et al. Rapidly recovering hydrogel scaffolds from self-assembling diblock copolypeptide amphiphiles. Nature. 2002; 417:424–428. [PubMed: 12024209]

26Anderson MA, et al. Astrocyte scar formation aids central nervous system axon regeneration. Nature. 2016; 532:195–200. [PubMed: 27027288]

27Yang CY, et al. Biocompatibility of amphiphilic diblock copolypeptide hydrogels in the central nervous system. Biomaterials. 2009; 30:2881–2898. [PubMed: 19251318]

Author Manuscript Author Manuscript Author Manuscript Author Manuscript

28Zhang S, et al. Thermoresponsive Copolypeptide Hydrogel Vehicles for Central Nervous System Cell Delivery. ACS Biomaterials Science & Engineering. 2015; 1:705–717. [PubMed: 27547820]

29Nicodemus GD, Bryant SJ. Cell Encapsulation in Biodegradable Hydrogels for Tissue Engineering Applications. Tissue Engineering Part B, Reviews. 2008; 14:149–165. [PubMed: 18498217]

30Deming TJ. Functional Modification of Thioether Groups in Peptides, Polypeptides, and Proteins. Bioconjugate Chemistry. 2017; 28:691–700. [PubMed: 28024390]

31Gundlach HG, Stein WH, Moore S. The nature of the amino acid residues involved in the inactivation of ribonuclease by iodoacetate. The Journal of biological chemistry. 1959; 234:1754–1760. [PubMed: 13672958]

32Perlmann GE, Katchalski E. Conformation of Poly-L-methionine and Some of its Derivatives in Solution. Journal of the American Chemical Society. 1962; 84:452–457.

33Kramer JR, Deming TJ. Preparation of Multifunctional and Multireactive Polypeptides via Methionine Alkylation. Biomacromolecules. 2012; 13:1719–1723. [PubMed: 22632141]

34Kim G, Weiss SJ, Levine RL. Methionine Oxidation and Reduction in Proteins. Biochimica et biophysica acta. 2014; 1840doi: 10.1016/j.bbagen.2013.1004.1038

35Brot N, Weissbach H. The biochemistry of methionine sulfoxide residues in proteins. Trends in Biochemical Sciences. 1982; 7:137–139.

36Vogt W. Oxidation of methionyl residues in proteins: tools, targets, and reversal. Free radical biology & medicine. 1995; 18:93–105. [PubMed: 7896176]

37Aiba SI, Minoura N, Fujiwara Y. Directional permeability of asymmetrically oxidized poly(L-methionine) film to oxygen dissolved in water. Journal of Applied Polymer Science. 1982; 27:1409–1411.

38Minoura N, Fujiwara Y, Nakagawa T. Permeability of poly-L-methionine membrane and its oxidized membrane to water vapor. Journal of Applied Polymer Science. 1978; 22:1593–1605.

39Pitha J, Szente L, Greenberg J. Poly-l-methionine Sulfoxide: A Biologically Inert Analogue of Dimethyl Sulfoxide with Solubilizing Potency. Journal of Pharmaceutical Sciences. 1983; 72:665–668. [PubMed: 6576129]

40Rodriguez AR, Kramer JR, Deming TJ. Enzyme-Triggered Cargo Release from Methionine Sulfoxide Containing Copolypeptide Vesicles. Biomacromolecules. 2013; 14:3610–3614. [PubMed: 23980867]

41Yamada S, Ikkyu K, Iso K, Goto M, Endo T. Facile synthesis of polymethionine oxides through polycondensation of activated urethane derivative of [small alpha]-amino acid and their application to antifouling polymer against proteins and cells. Polymer Chemistry. 2015; 6:1838–1845.

42Chapman RG, et al. Surveying for Surfaces that Resist the Adsorption of Proteins. Journal of the American Chemical Society. 2000; 122:8303–8304.

43Ostuni E, Chapman RG, Holmlin RE, Takayama S, Whitesides GM. A Survey of Structure −Property Relationships of Surfaces that Resist the Adsorption of Protein. Langmuir. 2001; 17:5605–5620.

44Gombotz WR, Guanghui W, Horbett TA, Hoffman AS. Protein adsorption to poly(ethylene oxide) surfaces. Journal of Biomedical Materials Research. 1991; 25:1547–1562. [PubMed: 1839026]

45Deng L, Mrksich M, Whitesides GM. Self-Assembled Monolayers of Alkanethiolates Presenting Tri(propylene sulfoxide) Groups Resist the Adsorption of Protein. Journal of the American Chemical Society. 1996; 118:5136–5137.

46Luk YY, Kato M, Mrksich M. Self-Assembled Monolayers of Alkanethiolates Presenting Mannitol Groups Are Inert to Protein Adsorption and Cell Attachment. Langmuir. 2000; 16:9604–9608.

47Mukkamala R, , Kushner AM, , Bertozzi CR. Polymer Gels Vol. 833. ACS Symposium Series; American Chemical Society; 2002163174 Ch. 11

48Brot N, Weissbach L, Werth J, Weissbach H. Enzymatic reduction of protein-bound methionine sulfoxide. Proceedings of the National Academy of Sciences. 1981; 78:2155–2158.

49Kramer JR, Deming TJ. General Method for Purification of α-Amino acid-N-carboxyanhydrides Using Flash Chromatography. Biomacromolecules. 2010; 11:3668–3672. [PubMed: 21047056]

50Deming TJ. Cobalt and Iron Initiators for the Controlled Polymerization of α-Amino Acid-N-Carboxyanhydrides. Macromolecules. 1999; 32:4500–4502.

Author Manuscript Author Manuscript Author Manuscript Author Manuscript

51Hernández JR, Klok HA. Synthesis and ring-opening (co)polymerization of L-lysine N-carboxyanhydrides containing labile side-chain protective groups. Journal of Polymer Science Part A: Polymer Chemistry. 2003; 41:1167–1187.

52Mavrogiorgis D, et al. Controlled polymerization of histidine and synthesis of well-defined stimuli responsive polymers. Elucidation of the structure-aggregation relationship of this highly multifunctional material. Polymer Chemistry. 2014; 5:6256–6278.

53Sun Y, et al. Conformation-Directed Formation of Self-Healing Diblock Copolypeptide Hydrogels via Polyion Complexation. Journal of the American Chemical Society. 2017; 139:15114–15121. [PubMed: 28976744]

54Sanz E, et al. Cell-type-specific isolation of ribosome-associated mRNA from complex tissues. Proceedings of the National Academy of Sciences. 2009; 106:13939–13944.

55Brown CR, Butts JC, McCreedy DA, Sakiyama-Elbert SE. Generation of V2a Interneurons from Mouse Embryonic Stem Cells. Stem Cells and Development. 2014; 23:1765–1776. [PubMed: 24650073]

56Roybon L, et al. Human Stem Cell-Derived Spinal Cord Astrocytes with Defined Mature or Reactive Phenotypes. Cell Reports. 2013; 4:1035–1048. [PubMed: 23994478]

57Wichterle H, Lieberam I, Porter JA, Jessell TM. Directed Differentiation of Embryonic Stem Cells into Motor Neurons. Cell. 2002; 110:385–397. [PubMed: 12176325]

58Krencik R, Weick JP, Liu Y, Zhang ZJ, Zhang SC. Specification of transplantable astroglial subtypes from human pluripotent stem cells. Nature Biotechnology. 2011; 29:528.

59Lutolf MP, Hubbell JA. Synthetic biomaterials as instructive extracellular microenvironments for morphogenesis in tissue engineering. Nature Biotechnology. 2005; 23:47.

60Guilak F, et al. Control of Stem Cell Fate by Physical Interactions with the Extracellular Matrix. Cell Stem Cell. 2009; 5:17–26. [PubMed: 19570510]

61Teixeira AI, Duckworth JK, Hermanson O. Getting the right stuff: Controlling neural stem cell state and fate in vivo and in vitro with biomaterials. Cell Research. 2007; 17:56. [PubMed: 17211445]

62Khakh BS, Sofroniew MV. Diversity of astrocyte functions and phenotypes in neural circuits. Nature neuroscience. 2015; 18:942–952. [PubMed: 26108722]

63Norris C, Kalil K. Guidance of callosal axons by radial glia in the developing cerebral cortex. The Journal of Neuroscience. 1991; 11:3481–3492. [PubMed: 1941093]

64Hasegawa K, et al. Embryonic radial glia bridge spinal cord lesions and promote functional recovery following spinal cord injury. Experimental Neurology. 2005; 193:394–410. [PubMed: 15869942]

65Chandrasekaran A, Avci HX, Leist M, Kobolák J, Dinnyés A. Astrocyte Differentiation of Human Pluripotent Stem Cells: New Tools for Neurological Disorder Research. Frontiers in Cellular Neuroscience. 2016; 10:215. [PubMed: 27725795]

66Chai H, et al. Neural Circuit-Specialized Astrocytes: Transcriptomic, Proteomic, Morphological, and Functional Evidence. Neuron. 2017; 95:531–549.e539. [PubMed: 28712653]

67Carmichael ST. The 3 Rs of Stroke Biology: Radial, Relayed, and Regenerative. Neurotherapeutics. 2016; 13:348–359. [PubMed: 26602550]

68O'Shea TM, Burda JE, Sofroniew MV. Cell biology of spinal cord injury and repair. Journal of Clinical Investigation. 2017; 127:3259–3270. [PubMed: 28737515]

Author Manuscript Author Manuscript Author Manuscript Author Manuscript

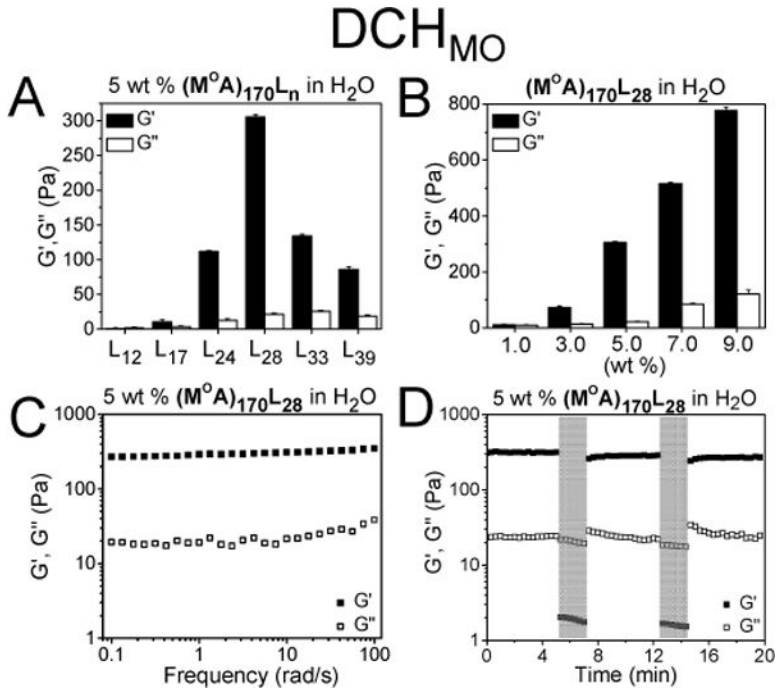

Figure 1. DCH$_{MO}$ mechanical properties evaluated by dynamic rheology

A) Storage modulus, G′ (Pa, black) and loss modulus, G″ (Pa, white) for **(M^{O}A)$_{170}$L$_n$** samples of different hydrophobic segment lengths (n = 12, 17, 24, 28, 33, and 39). All samples (5 wt %) were prepared in DI water at 25 °C. **B)** G′ (Pa, black) and G″ (Pa, white) for **(M^{O}A)$_{170}$L$_{28}$** at different concentrations in DI water at 25 °C. For **A)** and **B)** all G′ and G″ values were measured at an angular frequency of 10 rad/s and a percent strain of 0.5. Error bars represent the standard deviation for n = 3. **C)** G′ (Pa, filled squares) and G″ (Pa, open squares) for **(M^{O}A)$_{170}$L$_{28}$** at 5 wt % in DI water. G′ and G″ values were measured over an angular frequency range of 0.1 to 100 rad/s at a percent strain of 0.5. **D)** Recovery of a 5 wt % **(M^{O}A)$_{170}$L$_{28}$** hydrogel in DI water over time (G′, filled squares; G″, open squares) after application of stepwise large-amplitude oscillatory breakdown (gray area, percent strain of 1000 at 10 rad/s for 120 s) followed by low-amplitude linear recovery (white area, percent strain of 0.5 at 10 rad/s for 300 s).

Author Manuscript Author Manuscript Author Manuscript Author Manuscript

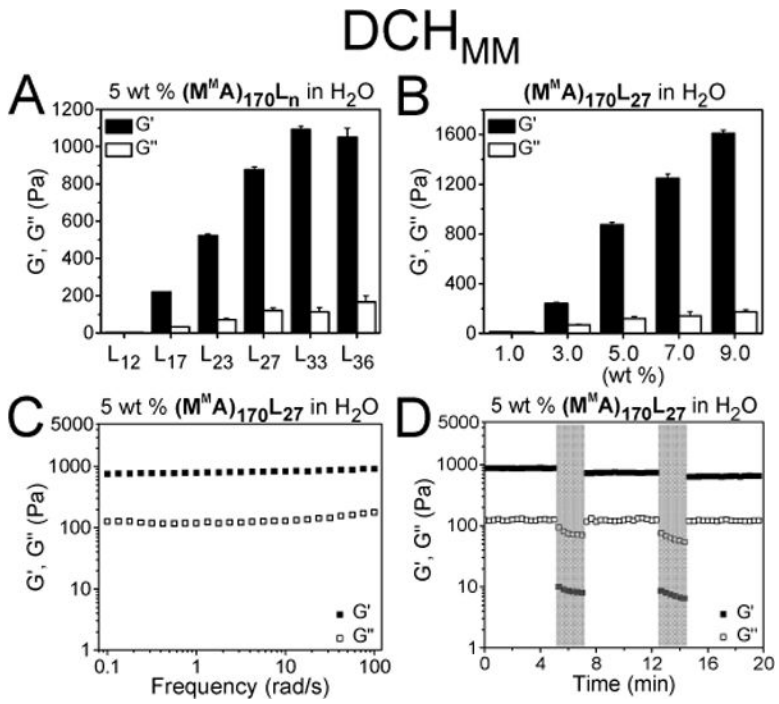

Figure 2. DCH$_{MM}$ mechanical properties evaluated by dynamic rheology

A) Storage modulus, G′ (Pa, black) and loss modulus, G″ (Pa, white) for **(M^{M}A)$_{170}$L$_n$** samples of different hydrophobic segment lengths (n = 12, 17, 23, 27, 33, and 36). All samples (5 wt %) were prepared in DI water at 25 °C. **B)** G′ (Pa, black) and G″ (Pa, white) for **(M^{M}A)$_{170}$L$_{27}$** at different concentrations in DI water at 25 °C. For **A)** and **B)** all G′ and G″ values were measured at an angular frequency of 10 rad/s and a percent strain of 0.5. Error bars represent the standard deviation for n = 3. **C)** G′ (Pa, filled squares) and G″ (Pa, open squares) for **(M^{M}A)$_{170}$L$_{27}$** at 5 wt % in DI water. G′ and G″ values were measured over an angular frequency range of 0.1 to 100 rad/s at a percent strain of 0.5. **D)** Recovery of a 5 wt % **(M^{M}A)$_{170}$L$_{27}$** hydrogel in DI water over time (G′, filled squares; G″, open squares) after application of stepwise large-amplitude oscillatory breakdown (gray area, percent strain of 1000 at 10 rad/s for 120 s) followed by low-amplitude linear recovery (white area, percent strain of 0.5 at 10 rad/s for 300 s).

Author Manuscript Author Manuscript Author Manuscript Author Manuscript

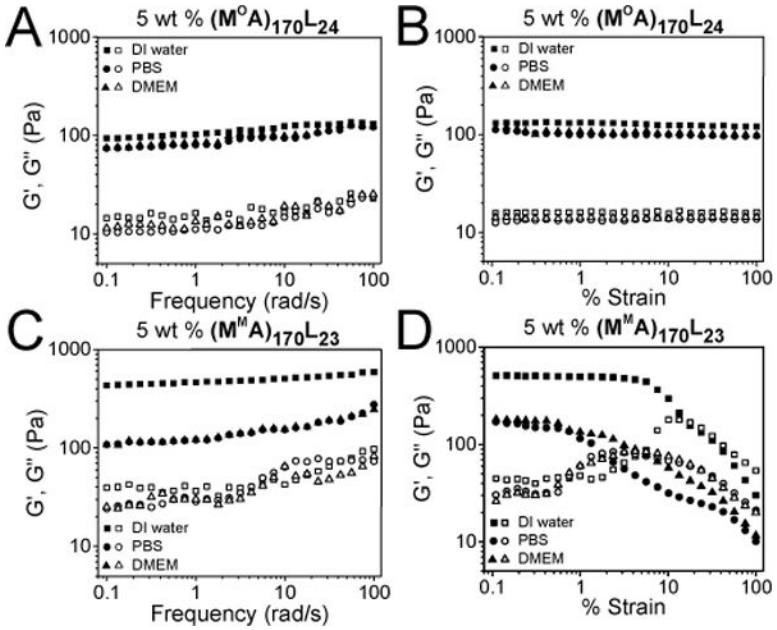

Figure 3. Effects of ionic media on DCH mechanical properties

DCH_{MO} and DCH_{MM} properties in DI water (squares), 1× PBS (circles), or DMEM (triangles). **A)** Storage modulus, G′ (Pa, filled symbols), and loss modulus, G″ (Pa, open symbols) versus frequency for 5 wt % $\mathbf{(M^{O}A)_{170}L_{24}}$ at 25 °C in different media. **B)** G′ (Pa, filled symbols), and G″ (Pa, open symbols) versus percent strain for 5 wt % $\mathbf{(M^{O}A)_{170}L_{24}}$ at 25 °C in different media. **C)** G′ (Pa, filled symbols), and G″ (Pa, open symbols) versus frequency for 5 wt % $\mathbf{(M^{M}A)_{170}L_{23}}$ at 25 °C in different media. **D)** G′ (Pa, filled symbols), and G″ (Pa, open symbols) versus percent strain for 5 wt % $\mathbf{(M^{M}A)_{170}L_{23}}$ at 25 °C in different media. For **A)** and **C)** G′ and G″ values were measured over an angular frequency of 0.1 to 100 rad/s at a percent strain of 0.5. For **B)** and **D)** G′ and G″ values were measured at an angular frequency of 10 rad/s over a percent strain of 0.1 to 100.

Author Manuscript Author Manuscript Author Manuscript Author Manuscript

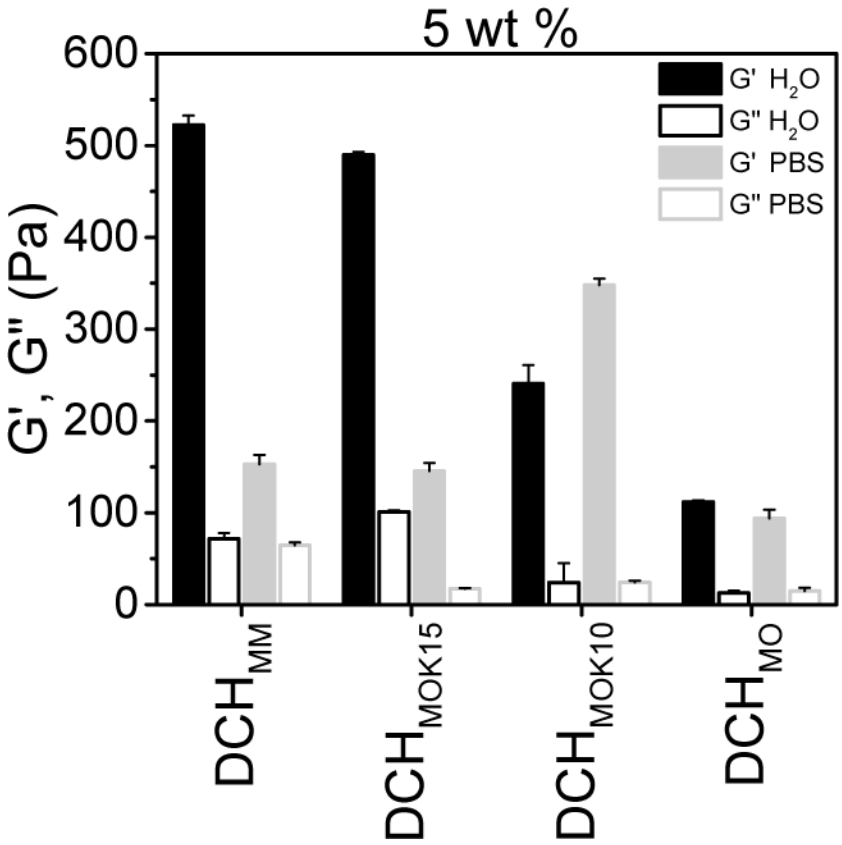

Figure 4. Effect of amino acid composition on DCH mechanical properties

Comparison of mechanical properties for DCH_{MM} ($\mathbf{(M^{M}A)_{170}L_{23}}$), DCH_{MO} ($\mathbf{(M^{O}A)_{170}L_{24}}$), DCH_{MOK10} ($\mathbf{(M^{O}_{0.90}K_{0.10})_{170}L_{23}}$), and DCH_{MOK15} ($\mathbf{(M^{O}_{0.85}K_{0.15})_{170}L_{23}}$) hydrogels. Hydrogels were prepared in either DI water (black bars) or 1× PBS (gray bars) at 5 wt %. Storage modulus G′ (Pa, filled bars) and loss modulus G″ (Pa, open bars) were measured at an angular frequency of 10 rad/s and a percent strain of 0.5 at 25 °C. Error bars represent the standard deviations for n = 3.

Author Manuscript Author Manuscript Author Manuscript Author Manuscript

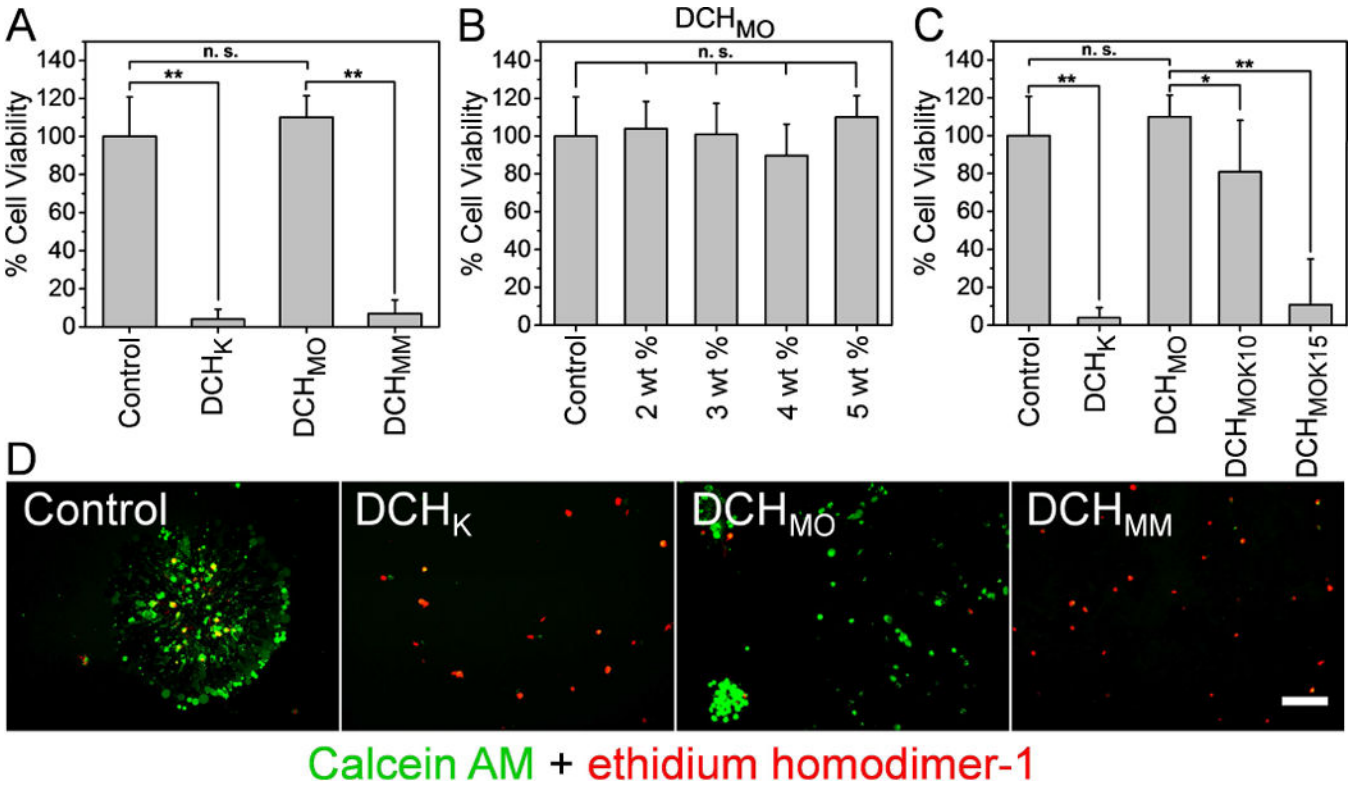

Figure 5. NSPC viability in Met based DCH

A-C) Quantification of cell viability of NSPCs in hydrogels demonstrates that DCH_{MO} is non-cytotoxic towards suspended NSPC across 2-5 wt% while cationic polypeptides are cytotoxic in a charge density dependent manner. **D)** Images of Calcein AM (Green - Live cell marker) and ethidium homodimer-1 (Red - dead cell marker) staining for NSPCs in various hydrogel formulations. Scale bar: 100 μm. Error bars are standard deviation of n = 15. Statistical tests: One-way Anova in **B)** and Welch's t-test in **A)** & **C)** were applied for comparison of means. P-values: * < 0.002 and ** < 0.0001.

Author Manuscript Author Manuscript Author Manuscript Author Manuscript

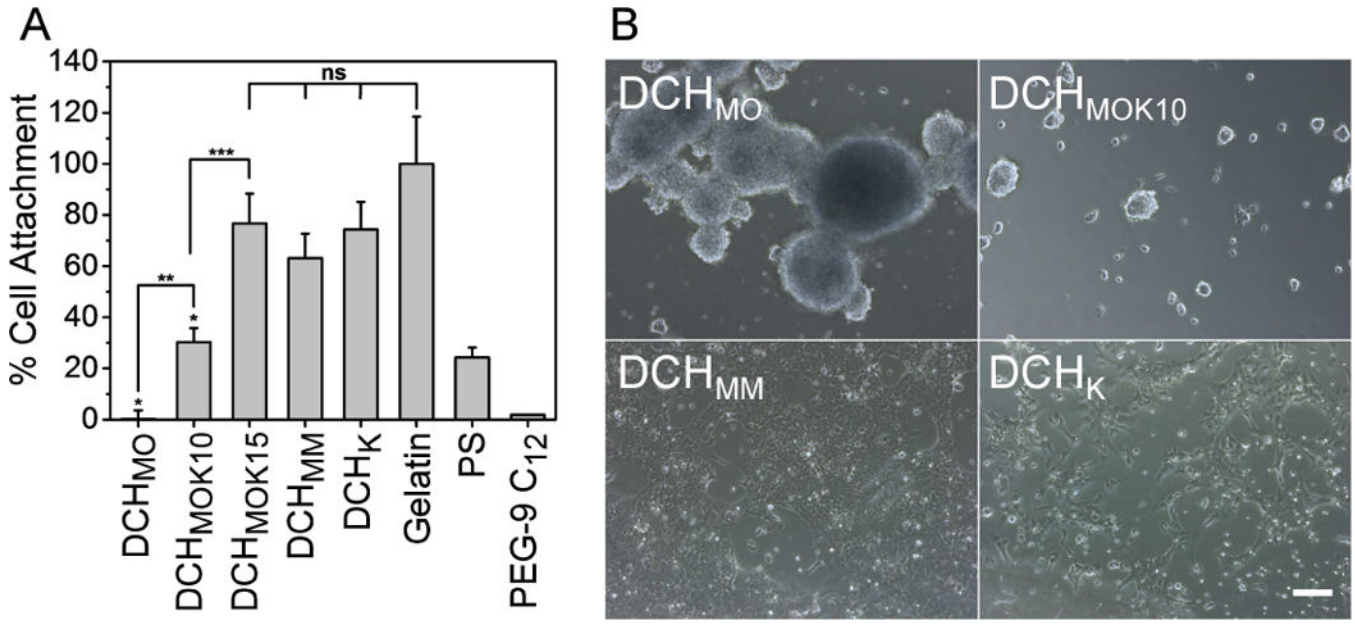

Figure 6. NSPC adhesion to Met based DCH

Untreated polystrene 96 well plates or hydrophobic glass slides were modified with different samples followed by seeding of NSPC. **A)** Quantification of NSPC attachment, as measured by fluorescent microplate measurements of Calcein AM staining, demonstrates the non-fouling properties of DCH_{MO} and the effect of polypeptide cationic charge on cell adhesion. Error bars are standard error of n = 12. Welch's t-tests were applied for the comparisons of individual DCH means compared to each other or compared to the Gelatin control. P-values: *< 0.003; **<0.002; ***< 0.0024. **B)** Brightfield microscope images of live NSPC on polypeptide coated hydrophobic glass substrates. NSPC seeded on DCH_{MO} do not adhere to the surface and instead form large multicellular aggregates. Scale bar: 100μm.

Author Manuscript Author Manuscript Author Manuscript Author Manuscript

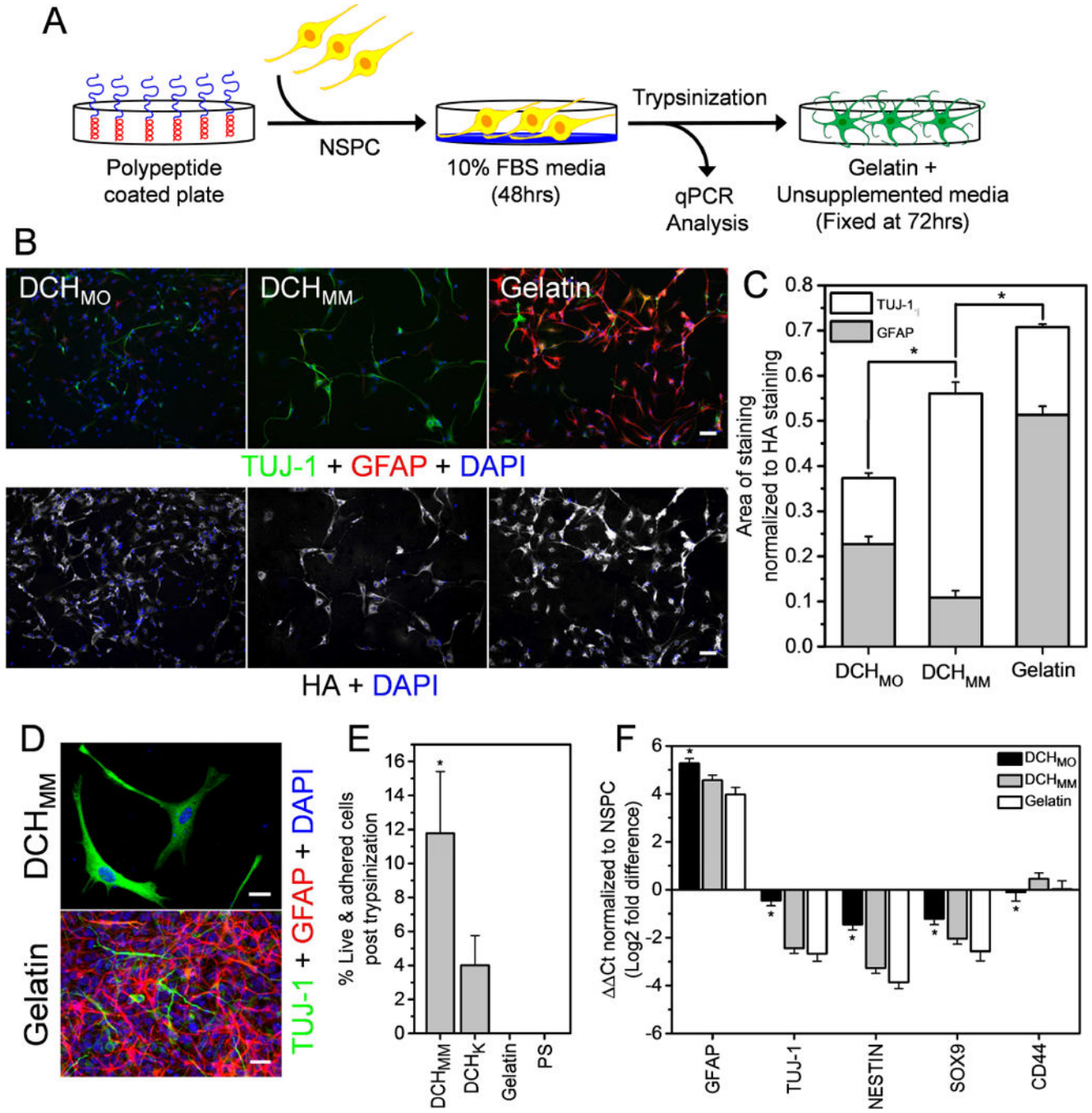

Figure 7. NSPC differentiation with Met Based DCH

A) Schematic outlining the *in vitro* culture assay to evaluate NSPC differentiation on various coated substrates. **B)** Immuno-histochemical staining of pan neuronal (TUJ-1-Green) and astrocyte (GFAP-Red) as well as whole cell staining by HA to evaluate NSPC differentiation on DCH_{MO}, DCH_{MM}, and Gelatin (Scale bar: 50μm). **C)** Quantification of Immunohistochemical staining for the different substrates reveals that DCH_{MO} promotes preserved NSPC multipotency. (n=28-30 images per group from 5 unique slides, error bars are represented as standard error or means. * P-value < 0.001). **D)** Immunohistochemical

Author Manuscript Author Manuscript Author Manuscript Author Manuscript

staining of TUJ-1 and GFAP on DCH_{MM} and Gelatin at the conclusion of FBS treatment (Scale bar: 20μm). **E)** Quantification of adhered viable cells remaining on coated surfaces after trypsinization reveals stronger cell attachment to DCH_{MM} compared to Gelatin (*P-value < 0.01). **F)** qPCR analysis of neural genes in NSPC samples seeded for 48hours on DCH_{MO}, DCH_{MM}, and Gelatin substrates in FBS containing medium (n=4, cDNA for each sample derived from mRNA collected by pooling of mRNA collected from cells from 3 unique experiments, * P-value < 0.03). Welch's t-tests were applied for the comparison of means throughout Figure 7.

Author Manuscript Author Manuscript Author Manuscript Author Manuscript

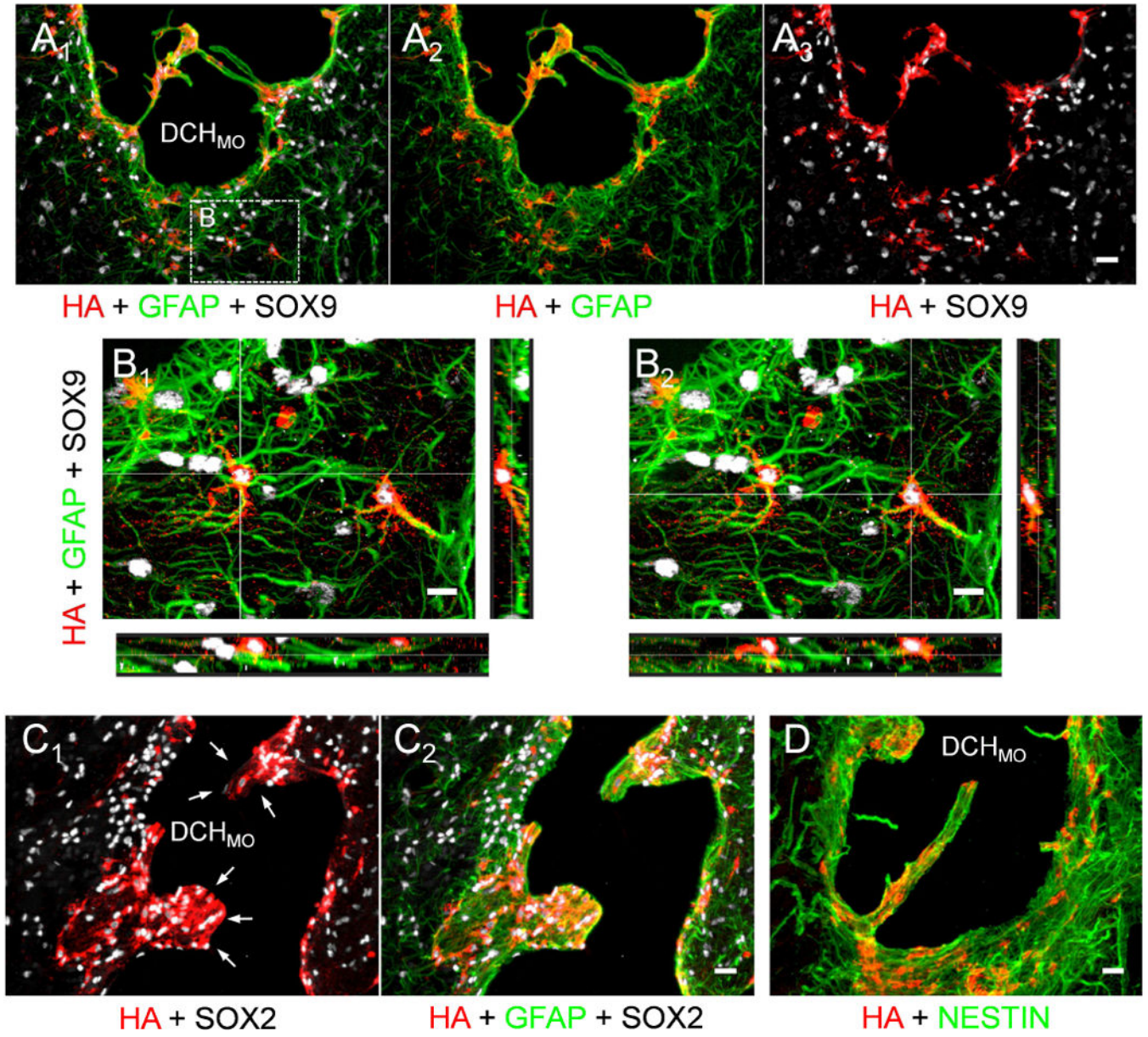

Figure 8. NSPC transplanted into healthy mouse brain using DCH_{MO} vehicle display an immature glial phenotype at 4 weeks

A) Immunohistochemical analysis of the DCH_{MO} + NSPC injection zone demonstrates abundant HA positive transplanted cells that robustly express GFAP and SOX9. **B)** High magnification and three-dimensional orthogonal-image of two unique HA positive cells that have integrated into healthy neural tissue and have adopted distinct, individual cellular domains. **C**) HA positive cells maintain robust expression of SOX2. Arrows in **C)** indicate transplanted neurospheres that have adhered to the margins of the DCH_{MO} deposit and integrated into host tissue. **D)** HA positive cells maintain robust expression of NESTIN. Scale bars in: **A)**, **C)** & **D)** are 25 μm; **B)** is 10 μm.

Author Manuscript Author Manuscript Author Manuscript Author Manuscript

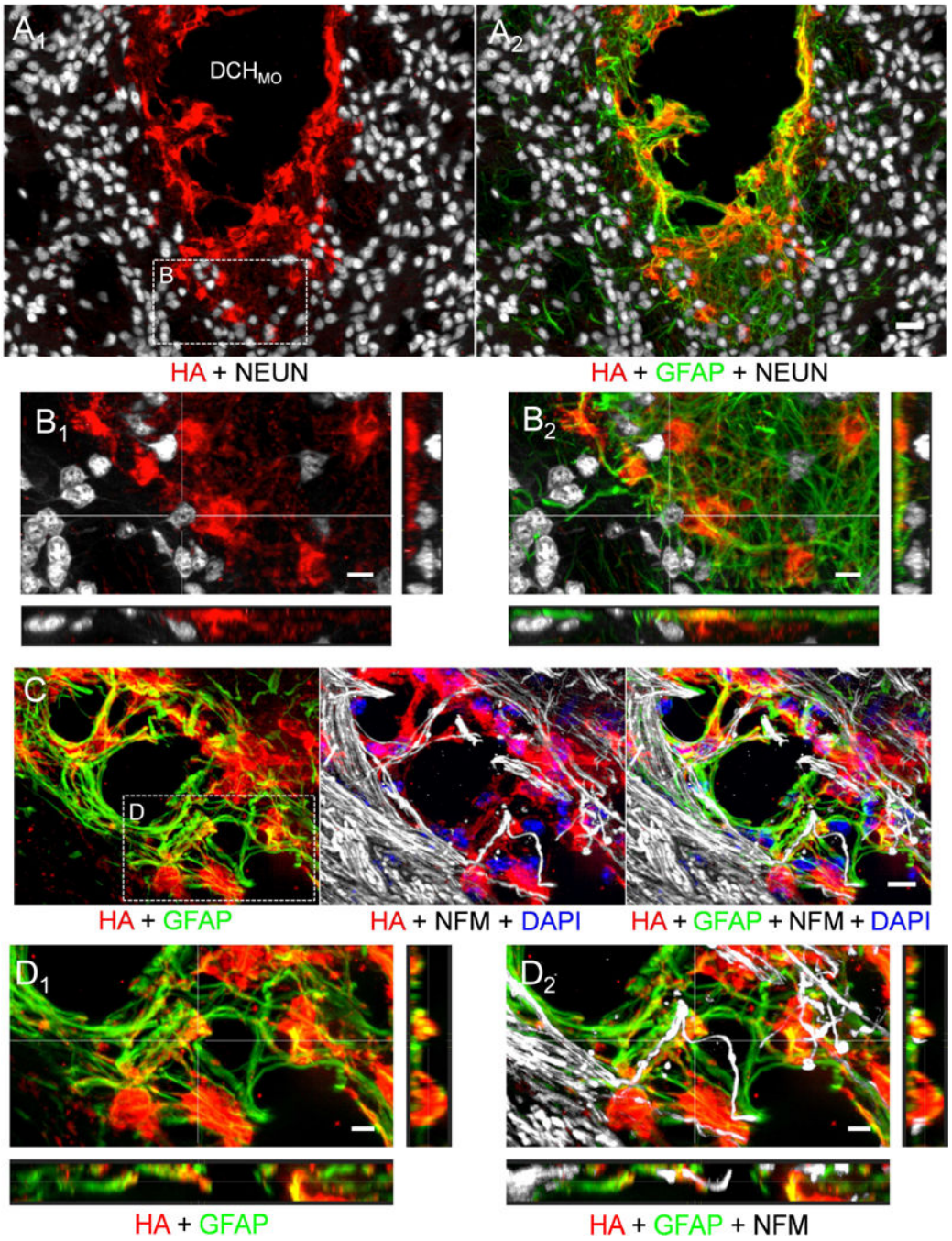

Figure 9. Transplanted NSPC interact with host neurons and provide cellular substrates for host axon growth

A) Immunohistochemical image showing integration of HA positive transplanted cells into host tissue with abundant NEUN positive neurons. **B)** High magnification image of a field from **A)** with a three dimensional orthogonal projection depicting HA positive cells interacting with NEUN positive neurons via GFAP positive cellular projections. **C)** Immunohistochemical image showing HA positive cells providing a cellular substrate for regrowth of axons that have been disrupted as a result of hydrogel injection. The torturous

growth projection of the axon stained with NFM is indicative of a newly regrowing or sprouted fiber. **D)** High magnification, three dimensional orthogonal projection showing NFM positive regrowing fibers in contact with a HA positive cells. Scale bars in: **A)** is 25 μm; **B)** & **C)** are 10 μm; and **D)** is 5 μm.

Author Manuscript Author Manuscript Author Manuscript Author Manuscript

Author Manuscript Author Manuscript Author Manuscript Author Manuscript

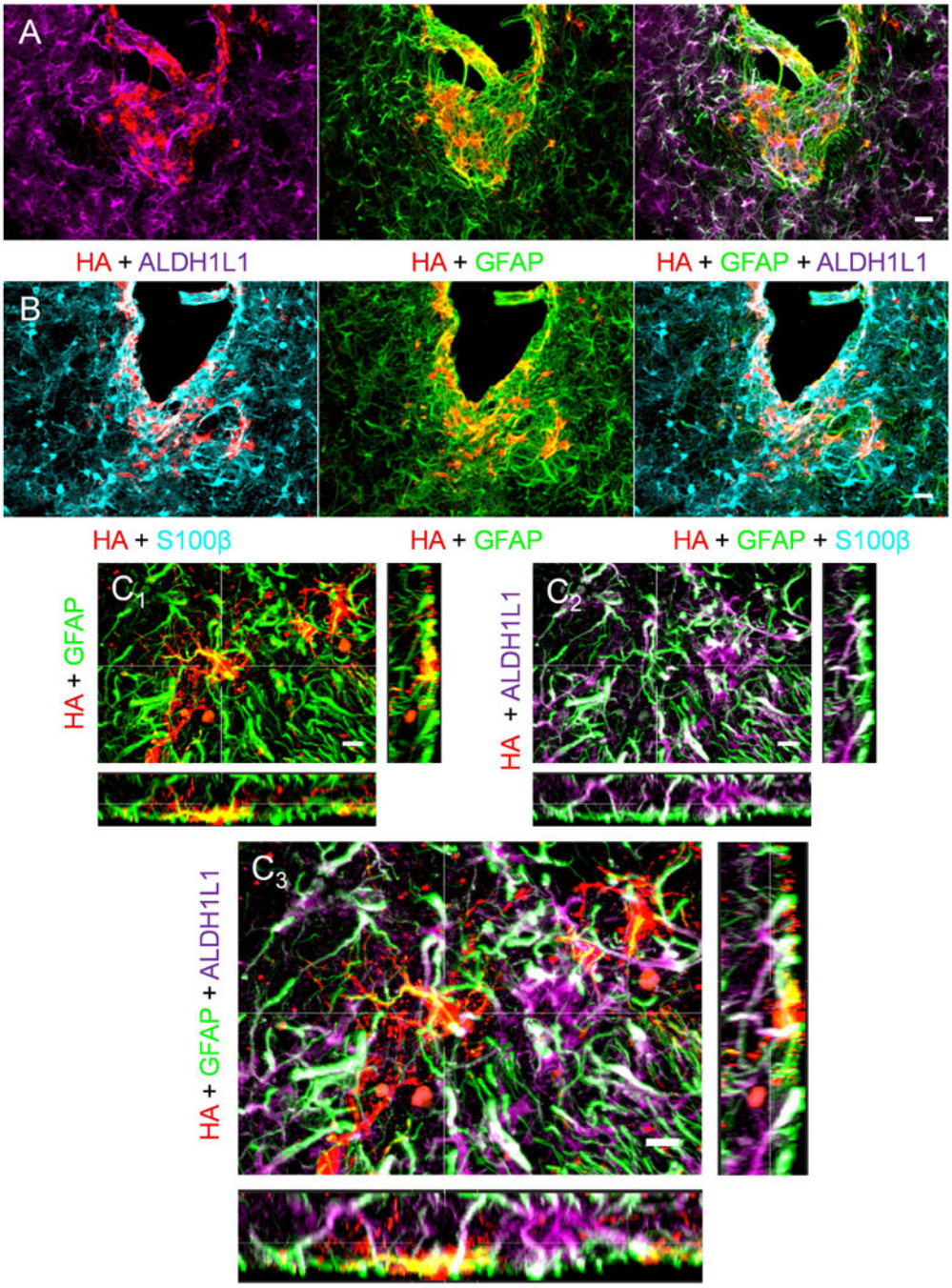

Figure 10. The progeny of transplanted NSPC do not express markers of mature astrocytes at 4 weeks but do interact directly with host mature astrocytes

A) Immunohistochemical image of HA positive cells intermingling with host astrocytes (GFAP & ALDH1L1 double positive cells). HA positive cells do not express ALDH1L1 and there are discrete regions of GFAP positive cells attributed to transplanted cells that do not express ALDH1L1. **B)** Some, but not all, HA positive cells express S100β as observed in the immunohistochemical image. White signal in **B)** indicates S100β and HA staining co-localization. **C)** High magnification, three dimensional orthogonal projection of HA &

Author Manuscript Author Manuscript Author Manuscript Author Manuscript

GFAP double positive transplanted cells interacting with an ALDH1L1 & GFAP double positive host astrocyte. In **C)** yellow staining is indicative of HA and GFAP co-localization while white staining is indicative of ALDH1L1 and GFAP co-localization. Scale bars in: **A)** & **B)** are 25 μm, **C**) is 10 μm.

Author Manuscript Author Manuscript Author Manuscript Author Manuscript

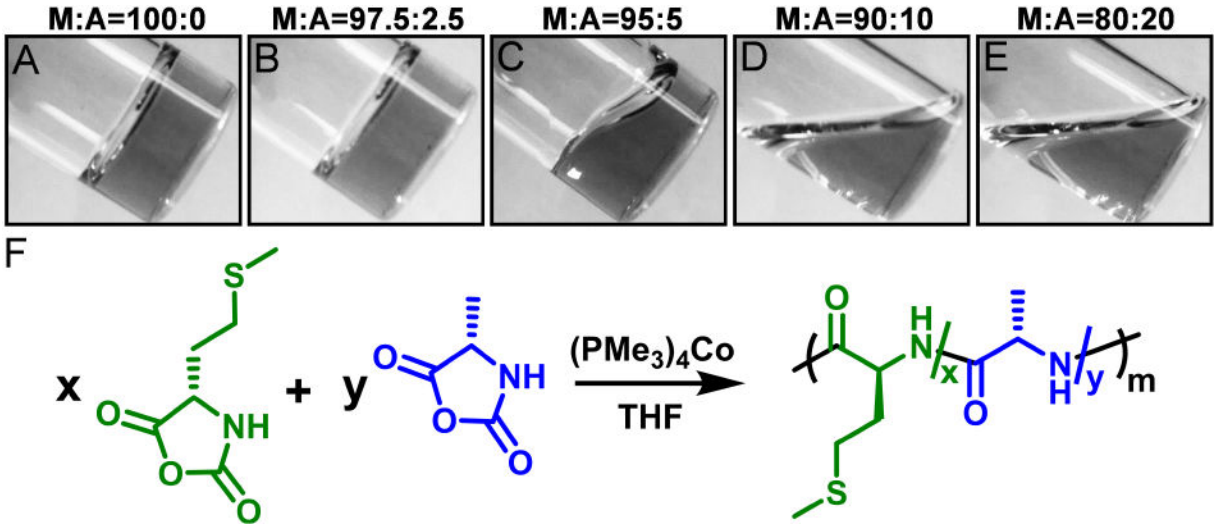

Scheme 1. Synthesis of MA statistical copolymers

Copolymerization of L-methionine NCA and L-alanine NCA with $Co(PMe_3)_4$ initiator to give **MA** copolymers in THF with a total NCA concentration of 50 mg/mL and total monomer to initiator ratio of 60:1. Images of reaction mixtures after complete monomer consumption were taken 30 seconds after tilting the vial to evaluate solution viscosity. **A) M**:**A** molar ratio = 100:0. **B) M**:**A** molar ratio = 97.5:2.5. **C) M**:**A** molar ratio = 95:5. **D) M**:**A** molar ratio = 90:10. **E) M**:**A** molar ratio = 80:20. **F)** Reaction scheme for the copolymerization of L-methionine and L-alanine NCAs. x = mole fraction **M**. y = mole fraction **A**. m = degree of polymerization.

Author Manuscript Author Manuscript Author Manuscript Author Manuscript

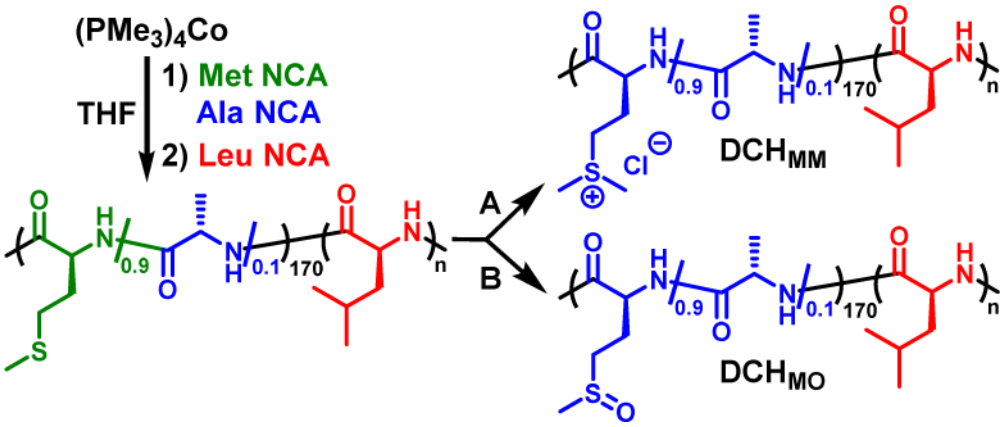

Scheme 2. Synthesis of modified methionine amphiphilic diblock copolypeptides

cationic $\mathbf{(M^{M}A)_{170}L_n}$ (DCH_{MM}) and nonionic $\mathbf{(M^{O}A)_{170}L_n}$ (DCH_{MO}). Reaction conditions: (A)MeI, H_2O, 20 °C, 5 d ; (B) TBHP, CSA, H_2O, 20 °C 1 d.

Author Manuscript Author Manuscript Author Manuscript Author Manuscript

Biomaterials. Author manuscript; available in PMC 2019 September 01.

Table 1

Copolymerization data for DCH_{MO} and DCH_{MM}.

	Sample	M_w/M_n [a]	Composition [b]	Yield [c] (%)	Functional Modification [d] (%)
DCH_{MO}	$M^O_{170}L_{23}$	1.28	$M^O_{176}L_{23}$	88.1	100
	$(M^OA)_{170}L_{12}$	1.44	$(M^OA)_{175}L_{12}$	84.3	100
	$(M^OA)_{170}L_{17}$	1.44	$(M^OA)_{164}L_{17}$	85.2	100
	$(M^OA)_{170}L_{24}$	1.44	$(M^OA)_{171}L_{24}$	84.6	100
	$(M^OA)_{170}L_{28}$	1.36	$(M^OA)_{167}L_{28}$	84.1	100
	$(M^OA)_{170}L_{33}$	1.33	$(M^OA)_{172}L_{33}$	85.6	100
	$(M^OA)_{170}L_{39}$	1.41	$(M^OA)_{164}L_{39}$	86.5	100
DCH_{MM}	$M^M_{170}L_{24}$	1.34	$M^M_{176}L_{24}$	88.7	98
	$(M^MA)_{170}L_{12}$	1.44	$(M^MA)_{179}L_{12}$	90.3	99
	$(M^MA)_{170}L_{17}$	1.35	$(M^MA)_{179}L_{17}$	88.8	99
	$(M^MA)_{170}L_{23}$	1.33	$(M^MA)_{178}L_{23}$	93.4	99
	$(M^MA)_{170}L_{27}$	1.34	$(M^MA)_{165}L_{27}$	92.7	99
	$(M^MA)_{170}L_{33}$	1.29	$(M^MA)_{165}L_{33}$	93.4	99
	$(M^MA)_{170}L_{36}$	1.25	$(M^MA)_{167}L_{36}$	93.4	98

[a] Dispersity values for **$(MA)_m$** copolypeptides were determined by GPC/LS.

[b] Amino acid compositions of diblock copolypeptides were determined by ^{1}H NMR integrations. Degree of polymerization of initial **$(MA)_m$** segment was determined by end-group analysis using ^{1}H NMR.

[c] Overall isolated yield of diblock copolypeptide after oxidation or alkylation of methionine residues.

[d] Percent functionalization after oxidation or alkylation reactions was determined using ^{1}H NMR.

Author Manuscript Author Manuscript Author Manuscript Author Manuscript

Table 2

Hydrogel formation of DCH_{MO} and DCH_{MM}.

	Sample	1 wt %	2 wt %	3 wt %	5 wt %	7 wt %	9 wt %
DCH_{MO}	$M^{O}_{170}L_{23}$						
	$(M^{O}A)_{170}L_{12}$						
	$(M^{O}A)_{170}L_{17}$						
	$(M^{O}A)_{170}L_{24}$						
	$(M^{O}A)_{170}L_{28}$						
	$(M^{O}A)_{170}L_{33}$				*	*	*
	$(M^{O}A)_{170}L_{39}$			*	*	*	*
DCH_{MM}	$M^{M}_{170}L_{24}$						*
	$(M^{M}A)_{170}L_{12}$						
	$(M^{M}A)_{170}L_{17}$						
	$(M^{M}A)_{170}L_{23}$					*	*
	$(M^{M}A)_{170}L_{27}$				*	*	*
	$(M^{M}A)_{170}L_{33}$			*	*	*	*
	$(M^{M}A)_{170}L_{36}$			*	*	*	*

Properties of DCH_{MO} and DCH_{MM} samples after dispersion in DI H_2O at different concentrations. Samples were found to be either clear liquids (gray box), clear hydrogels (white box), or opaque hydrogels (*).